Graphene Oxide Elicits Membrane Lipid Changes and Neutrophil Extracellular Trap Formation

Chem

CellPress

Article

Graphene Oxide Elicits Membrane Lipid Changes and Neutrophil Extracellular Trap Formation

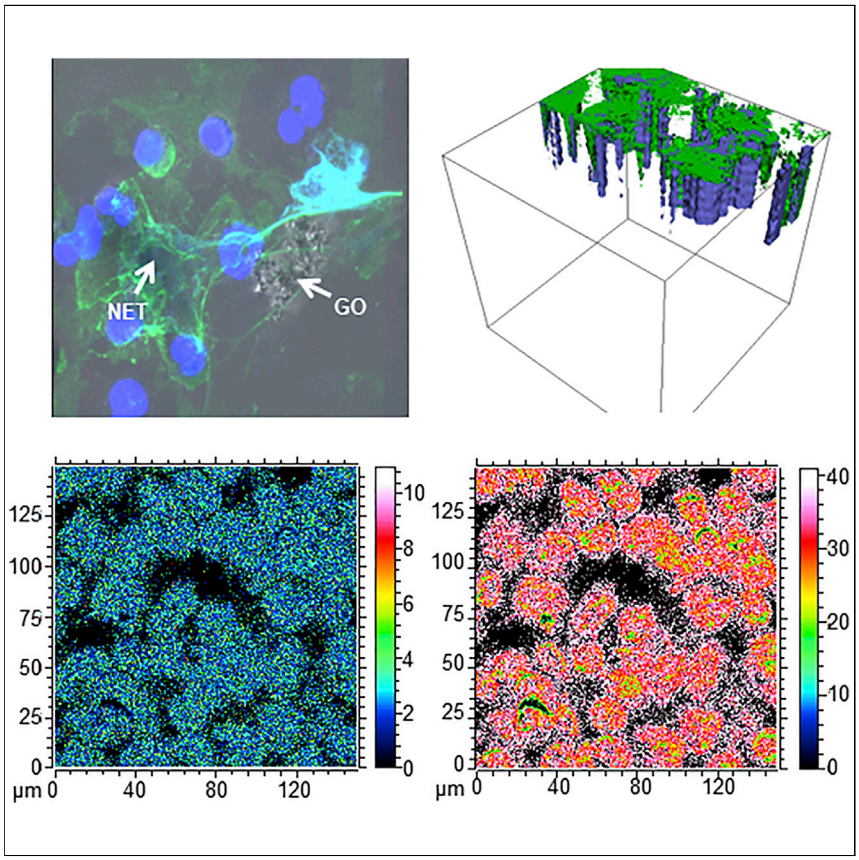

Graphene oxide (GO) is a promising material for a variety of biomedical and other applications. The increasing use of GO necessitates careful assessment of potential health hazards. Using primary neutrophils as a model, Mukherjee et al. show that GO elicits neutrophil extracellular traps. Furthermore, by using ToF-SIMS, the authors noted pronounced perturbations of plasma membrane lipids in cells exposed to GO.

Sourav P. Mukherjee, Beatrice Lazzaretto, Kjell Hultenby, ..., Kostas Kostarelos, Per Malmberg, Bengt Fadeel

bengt.fadeel@ki.se

HIGHLIGHTS

Graphene oxide (GO) triggers the release of neutrophil extracellular traps (NETs)

Size-dependent induction of NETs is associated with ROS production and Ca^{2+} influx

GO causes a disruption of lipid raft domains in the plasma membrane of neutrophils

GO elicits pronounced alterations of plasma membrane lipids, including cholesterol

Mukherjee et al., Chem 4, 334–358
February 8, 2018
https://doi.org/10.1016/j.chempr.2017.12.017

Chem

CellPress

Article

Graphene Oxide Elicits Membrane Lipid Changes and Neutrophil Extracellular Trap Formation

Sourav P. Mukherjee,[1] Beatrice Lazzaretto,[1] Kjell Hultenby,[2] Leon Newman,[3] Artur F. Rodrigues,[3] Neus Lozano,[3] Kostas Kostarelos,[3] Per Malmberg,[4] and Bengt Fadeel[1,5,*]

SUMMARY

Understanding the biological interactions of graphene-based materials is important for the safe use of these materials. Previous studies have explored the interaction between graphene oxide (GO) and macrophages but not the impact of GO on neutrophils, key cells of the immune system. Here, we synthesized GO sheets with differing lateral dimensions and showed by using an array of analytical and imaging techniques, including transmission and scanning electron microscopy, confocal microscopy, and time-of-flight secondary ion mass spectroscopy (ToF-SIMS), that GO elicited the formation of neutrophil extracellular traps (NETs). ToF-SIMS revealed pronounced perturbations of plasma membrane lipids, including a decrease in cholesterol and increased levels of oxidized cholesterol species. The induction of NETs was size dependent and associated with the production of mitochondrial reactive oxygen species and calcium influx. Importantly, antioxidant treatment reduced the production of NETs. These studies provide evidence that a previously undescribed biological effect of GO manifests through direct effects on membrane lipids.

INTRODUCTION

Graphene and its derivatives have received considerable attention in recent years in numerous sectors of science and technology.[1] Graphene oxide (GO), in particular, is currently being investigated for various biomedical applications such as drug delivery and medical imaging.[2,3] The application of graphene-based materials in the clinic requires careful assessment of their biocompatibility and a detailed understanding of their cellular interactions.[4] Moreover, safety assessment is mandatory not only in the clinical setting but also at all stages of the life cycle of the material, including its production, use, and disposal.[5] Determining potential interactions with the immune system, our first line of defense against foreign intrusion, is of particular importance. Considerable efforts have been invested in elucidating the interaction of carbon-based nanomaterials such as single- and multi-walled carbon nanotubes (CNTs) with cells of the immune system,[6,7] and recent work has shown that these interactions may be reciprocal; hence, CNTs may trigger inflammation, involving macrophages, neutrophils, and other cell types, but inflammatory cells including neutrophils can also strike back and digest CNTs through an enzymatic, oxidative reaction,[8] which may serve to mitigate the inflammatory potential of these materials.[9] However, for graphene-based materials, there is a paucity of data with regard to their potential immunotoxicity.[10] Previous animal studies have shown that GO is pro-fibrogenic after oropharyngeal instillation,[11] and GO was found to modulate immune responses in a mouse model of asthma,[12] but there is still a

The Bigger Picture

Graphene oxide (GO) is being investigated for various biomedical applications. Understanding the interactions between GO and living cells is of critical importance for the safe use of these materials in patients. In the present study, we identified effects of GO on neutrophils, the most common type of white blood cell. We first synthesized GO sheets of different sizes and carefully characterized the materials. Then, using various analytical and imaging techniques, we found that GO triggered so-called neutrophil extracellular traps or NETs. NETs are normally deployed by neutrophils to capture and destroy pathogens. We were able to show that GO caused significant changes in the lipid composition of the neutrophil cell membrane, whereby the oxidation of cholesterol set into motion a cascade of intracellular events leading to the formation of NETs. These studies show that GO acts directly on the neutrophil cell membrane and leads to the activation of a conserved anti-pathogen response.

lack of systematic studies of graphene of different lateral dimensions, different number of layers, or degree of oxidation.[13] Such studies are needed for assigning a toxicological outcome, if any, to specific material properties.

Neutrophils or polymorphonuclear granulocytes are major players in inflammation.[7] They are typically the first cells to be recruited to an inflammatory site and are capable of eliminating pathogens by multiple mechanisms. Hence, neutrophils are equipped with oxidative and proteolytic enzymes for the destruction of ingested pathogens. Neutrophils also undergo degranulation to release antimicrobial factors, and they release so-called neutrophil extracellular traps or NETs, which contribute to the defense against extracellular pathogens.[14] NETs consist of chromatin fibers decorated with antimicrobial proteins, including neutrophil elastase (NE) and myeloperoxidase (MPO). The release of NETs is often associated with cell death (so-called NETosis), even though some studies have shown that neutrophils may continue to perform certain functions, including chemotaxis and phagocytosis, after producing NETs.[15] Increasing evidence suggests that the release of NETs might also occur in noninfectious, sterile inflammation and may contribute to tissue damage.[16] For instance, previous studies have shown that crystals of monosodium urate, the causative agent of gout, induced neutrophils to release NETs.[17] Furthermore, in a recent study, 10–40 nm polystyrene nanoparticles and nanodiamonds triggered a self-limiting NETosis-driven inflammation.[18] The authors presumed that the effects were mediated via interactions of the hydrophobic nanoparticles with plasma membrane lipids, but experimental evidence for this was not presented. No NET formation was seen when cells were incubated with micrometer-sized particles.[18] Other studies have suggested that gold nanoparticles trigger the formation of extracellular structures or traps.[19] However, detection of extracellular DNA is not a specific marker of NETs because DNA release may also occur during late stages of cell death, and other markers such as NE are required.[16]

In recent years, the view has emerged that nanomaterials are endowed with a new biological identity as soon as they come into contact with biological fluids,[20] and this so-called bio-corona was shown to influence the biological effects of nanoparticles.[21] Recent *in vitro* studies have shown that the adsorption of serum proteins onto the surface of CNTs and GO serves to reduce their cytotoxicity,[22,23] and previous work showed that the adsorption of a lung surfactant corona of proteins and lipids markedly enhanced macrophage uptake of CNTs.[24] However, these studies were designed to assess the impact of a pre-formed corona of proteins and/or lipids on nanomaterial-cell interactions. Studies on the possibility of direct nanomaterial interactions with proteins or lipids in the plasma membrane are also emerging, although few studies to date have addressed direct interactions of nanomaterials with membranes of intact cells. The plasma membrane consists of a lipid bilayer with embedded proteins, and it separates the cell interior from the external environment; it also serves as an important site for cell-cell signaling. In a recent study published in *Chem*, using confocal and scanning electron microscopy, Sun et al.[25,26] found that GO triggered membrane ruffling in a variety of different cell lines, albeit in the absence of cell death. Furthermore, Tu et al.[27] noted signs of membrane damage in *Escherichia coli* incubated with nano-sized GO. The authors applied molecular dynamics (MD) simulations by using two phospholipids found in Gram-negative bacteria, palmitoyloleoylphosphatidylethanolamine and palmitoyloleoylphosphatidylglycerol, and found evidence of lipid extraction by GO.[27] Chen et al.[28] recently reported, on the basis of MD simulations, that pristine graphene can penetrate into a model lipid membrane and has no effect on the integrity of the membrane, whereas GO is embedded into the membrane and can extract lipid molecules,

[1]Nanosafety & Nanomedicine Laboratory, Division of Molecular Toxicology, Institute of Environmental Medicine, Karolinska Institutet, 171 77 Stockholm, Sweden

[2]Clinical Research Center, Department of Laboratory Medicine, Karolinska Institutet, Karolinska University Hospital Huddinge, 141 85 Stockholm, Sweden

[3]Nanomedicine Laboratory, Faculty of Biology, Medicine, and Health and National Graphene Institute, University of Manchester, Manchester M13 9PT, UK

[4]Department of Chemistry and Chemical Engineering, Chalmers University of Technology and National Center for Imaging Mass Spectrometry, 412 96 Gothenburg, Sweden

[5]Lead Contact

*Correspondence: bengt.fadeel@ki.se

https://doi.org/10.1016/j.chempr.2017.12.017

resulting in pore formation. Similar results, from MD simulations, were reported by Duan et al.[29] who also provided evidence for the formation of pores in the plasma membrane of cell lines exposed to very high doses (200 μg/mL) of single-layered GO with lateral dimensions of 200–700 nm; it was proposed that the pore formation was driven by lipid extraction. In addition, studies using supported lipid bilayers and liposomes have demonstrated that GO interacts with and disrupts lipid membranes.[30,31] However, whether lipid extraction or other perturbations of membrane lipids occur in living cells exposed to GO has not been demonstrated experimentally. Here, we studied the effect of GO of differing lateral dimensions on primary human neutrophils and found that GO induces loss of cell viability with the release of NETs. By using time-of-flight secondary ion mass spectroscopy (ToF-SIMS), we observed direct evidence of lipid perturbations in the plasma membrane of GO-exposed cells. We were able to show that the induction of NETs is size dependent and that antioxidant treatment reduces NET formation. These studies further our understanding of the biological interactions of GO and point to a novel mechanism of toxicity involving neutrophils, the most abundant type of white blood cell.

RESULTS AND DISCUSSION

Preparation and Characterization of GO

To assess the role of the lateral size of GO for cellular interactions, we prepared GO samples containing sheets with differing lateral dimensions by the modified Hummer's method as previously described[32] and subjected the samples to exhaustive characterization. The lateral dimensions and thickness of the samples were analyzed by transmission electron microscopy (TEM) and atomic force microscopy (AFM) (Figures 1A and 1B). The lateral size distribution of small and large GO is shown in Figure 1C. AFM revealed that small (GO-S) and large (GO-L) sheets were one or two layers thick (1–2 nm), and both GO samples had strongly negative charge (average ζ potential −55 mV) because of the multiple surface oxygen groups (Figure 1D). Raman spectroscopy showed characteristic D and G bands at 1,319 and 1,596 cm^{-1}, respectively (Figure S1A). Thermo-gravimetric analysis (TGA) (Figure S1B) and X-ray photoelectron spectroscopy (XPS) (Figure S1C) were performed to quantify the oxidation degree and purity of the GO samples (>99.5%) (see Table S1 for a summary of the characterization results). Thus, small (50–300 nm) and large (10–40 μm) GO samples of one to two layers were produced without any significant differences in their surface properties. Moreover, the dispersion of GO in cell culture medium did not change the morphology of GO significantly (Figure S2A), although some agglomeration was identified by dynamic light scattering (DLS) (Figure S2B). Both GO samples exhibited a similar colloidal stability in cell culture medium (average ζ potential −37 mV).

Endotoxin contamination of carbon-based nanomaterials may result in potential artifacts, which could skew the results when studying effects on immune-competent cells.[33] We have recently reported that graphene-based materials may interfere with traditional endotoxin tests.[34] Therefore, we assessed the as-synthesized GO samples for potential endotoxin contamination by using a newly developed macrophage activation test based on primary human macrophages[34] and showed that both GO samples were endotoxin free (Figure 1E). Lipopolysaccharide (LPS) was included as a positive control, and LPS-induced tumor necrosis factor alpha (TNF-α) secretion was blocked by the specific LPS inhibitor, polymyxin B (10 μM).

GO Triggers Neutrophil Extracellular Traps

Previous studies showed that small and large GO sheets were non-cytotoxic for peripheral blood mononuclear cells (PBMCs) from healthy donors that included

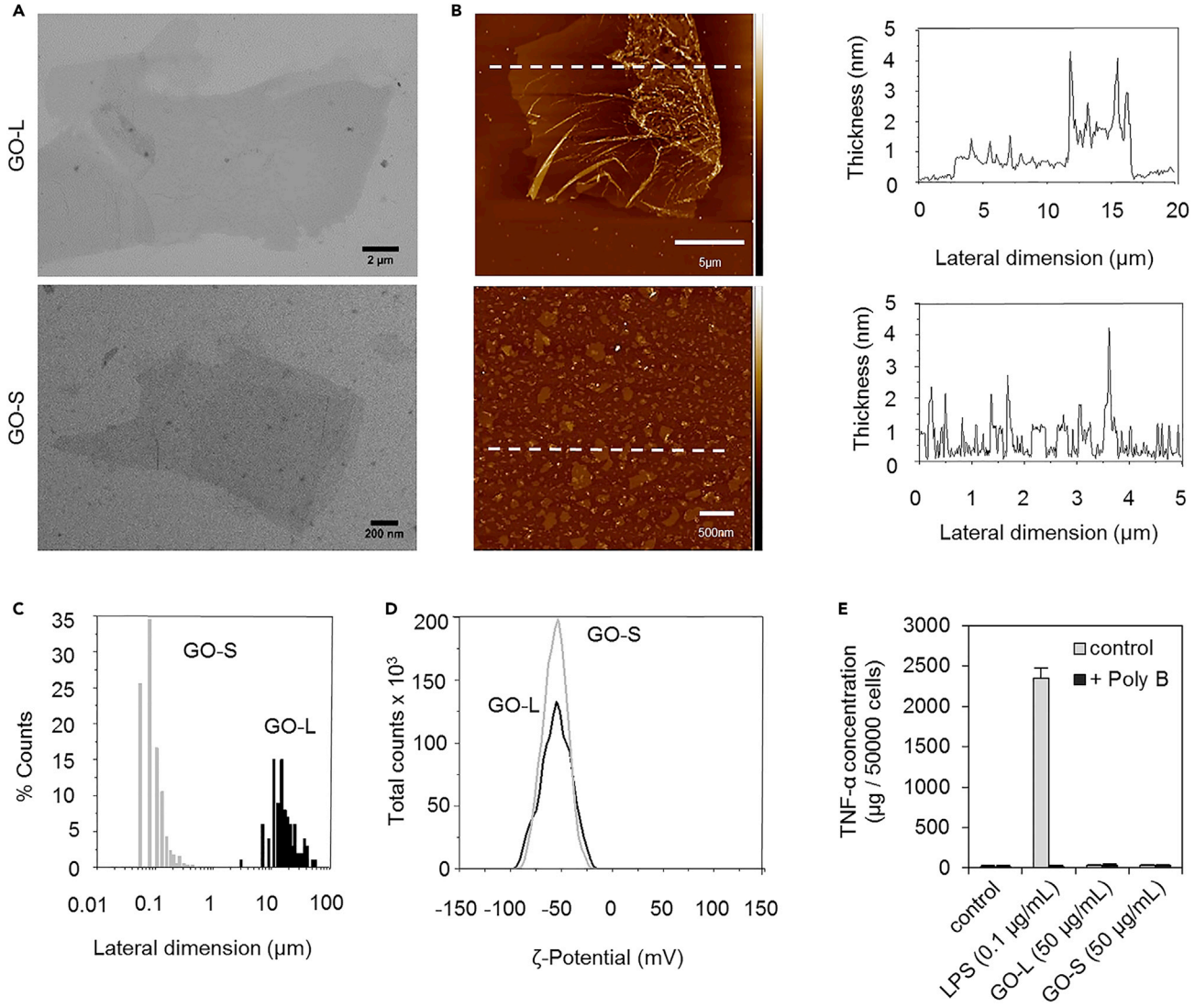

Figure 1. Characterization of Small and Large GO Sheets

(A) TEM micrographs of GO-L (large) and GO-S (small). Scale bars: 2 μm (GO-L) and 200 nm (GO-S).

(B) AFM of GO-L and GO-S: height images (left) and thickness analysis from the cross-section (right). Scale bars: 5 μm (GO-L) and 500 nm (GO-S).

(C) Lateral dimension distribution analysis of GO-L and GO-S.

(D) Measurements of zeta potential. Refer to Figure S1 and Table S1 for further characterization of GO-S and GO-L samples.

(E) Endotoxin content was assessed on the basis of TNF-α secretion by primary human macrophages exposed to GO with or without the LPS inhibitor, polymyxin B. LPS served as positive control. Data are shown as mean values ± SEM.

T cells, B cells, monocytes, dendritic cells (DCs), and natural killer cells.[35] The only exception was noted when PBMCs were exposed to high doses (75 μg/mL) of small GO sheets (up to 20% loss of cell viability). However, to our knowledge, there are no studies to date on the potential impact of GO on polymorphonuclear neutrophils, key players of the innate immune system. We therefore proceeded to test the effect of small versus large GO on primary human neutrophils freshly isolated from healthy human blood donors by using established protocols. Neutrophils are short-lived cells and are known to undergo spontaneous apoptosis upon *ex vivo* culture,[36] and for this reason, all experiments were conducted within a 2–3 hr time frame after isolation of the cells from peripheral blood. GO triggered a dose-dependent loss of cell viability in neutrophils (Figure 2A). The phorbol ester

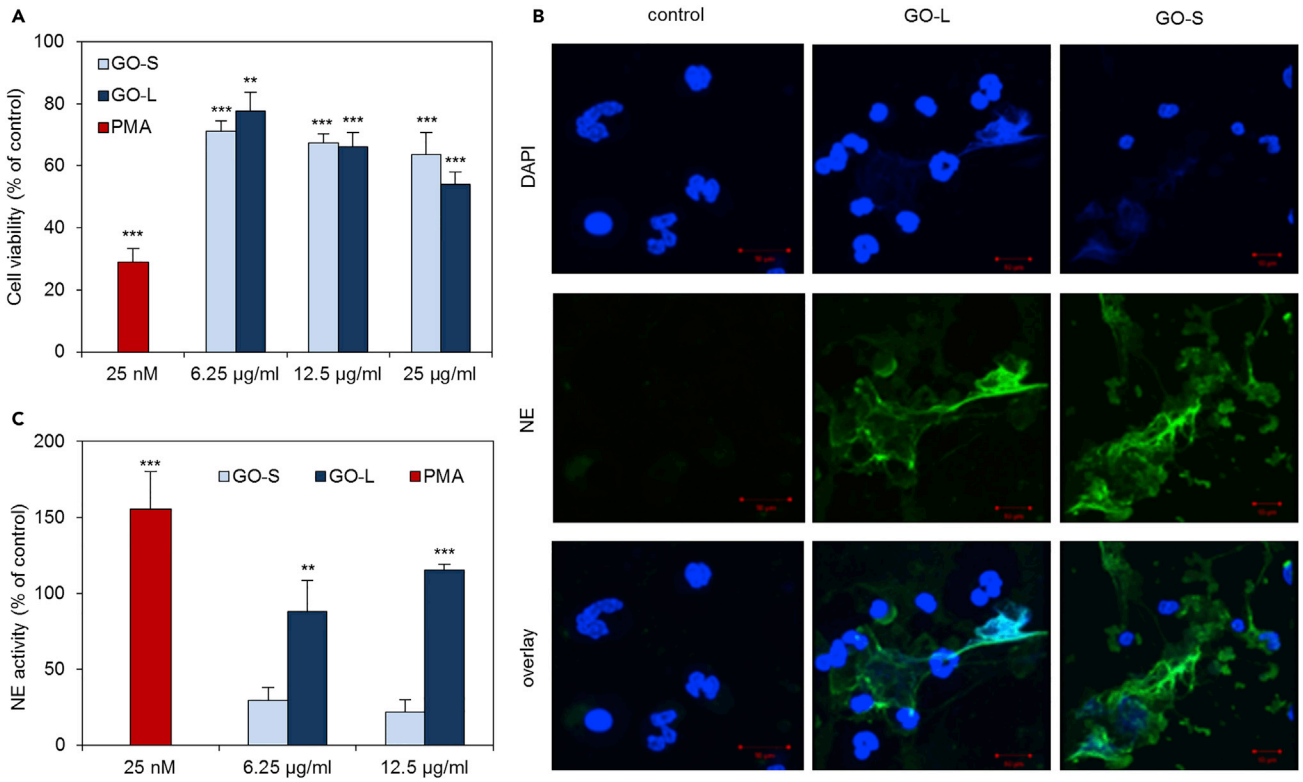

Figure 2. GO Triggers Neutrophil Extracellular Traps

(A) Cell viability as determined by a luminescence-based assay for quantification of cellular ATP. Freshly isolated primary human neutrophils were incubated with GO-L or GO-S (12.5 µg/mL) for 3 hr. PMA was included as positive control. Data are shown as mean values ± SEM. **p < 0.01; ***p < 0.001.

(B) Confocal imaging of neutrophils incubated in medium alone or in the presence of GO-L or GO-S (12.5 µg/mL) for 2 hr. Cells were stained with specific antibodies to neutrophil elastase (NE) followed by a secondary FITC-labeled antibody (green) and counterstained with DAPI (blue) for visualization of DNA. Scale bars: 10 µm.

(C) Size-dependent induction of NETs by GO as demonstrated by the quantification of extracellular NE activity. PMA was included as positive control. **p < 0.01; ***p < 0.001.

phorbol-12-myristate-13-acetate (PMA) (25 nM) was included as a positive control.[36] Next, we performed TEM imaging of neutrophils exposed for 2 hr to small versus large GO (12.5 µg/mL). TEM showed that some GO was internalized by the cells; however, GO also appeared to interact with the plasma membrane of the cells; evidence of membrane "stripping" was seen in particular for the large GO sheets (Figure S3). Previous studies using macrophages have shown that large GO sheets (~1 µm in lateral size) might align with the plasma membrane and thereby lead to a "masking" effect, whereas smaller GO sheets were more likely to be taken up by the cells.[37,38] However, the majority of these studies were conducted with murine or human cell lines and not with primary, professional phagocytes. The present electron microscopy results suggested that GO could elicit membrane stripping instead of membrane masking in primary human neutrophils. To further characterize the effect of GO on neutrophils, we performed scanning electron microscopy (SEM) after a 2 hr exposure to small versus large GO (12.5 µg/mL). PMA (25 nM) was used as a positive control. Figure 3A (low-magnification view) and Figure 3B (high-magnification view) show that PMA triggered the formation of NETs, as previously reported.[39] Remarkably, large GO also triggered the production of NETs (Figure 3A), and some GO sheets were found trapped in the NETs (Figure 3B, arrow). Moreover, small GO also triggered NETs (Figure 3A), and these NETs were apparently coated with

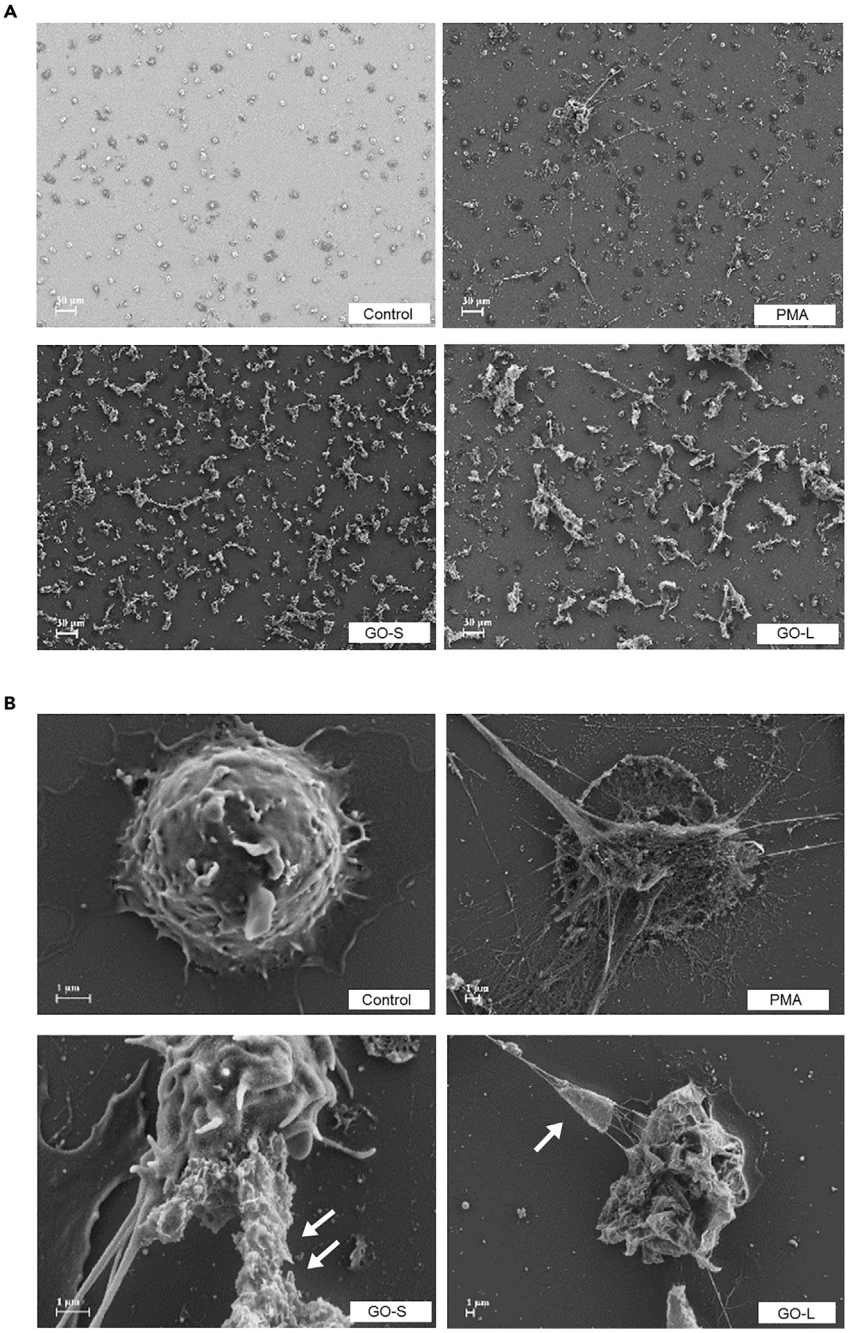

Figure 3. Small and Large GO Sheets Trigger NETs

Low-magnification (A) and high-magnification (B) SEM micrographs of control neutrophils or neutrophils exposed to PMA (25 nM), GO-L (12.5 μg/mL), or GO-S (12.5 μg/mL). The single arrow (B) points to a large GO sheet entrapped in a network of chromatin fibers (i.e., NETs). The pair of arrows (B) indicates chromatin fibers (NETs) coated with small GO sheets. Scale bars: 30 μm (A) and 1 μm (B).

GO, as shown in Figure 3B. In contrast, our previous work showed that short, oxidized single-walled CNTs were trapped in NETs produced by PMA-stimulated neutrophils but failed to trigger a significant induction of NETs themselves.[40] One may ask how negatively charged GO (or CNTs) are attracted to NETs whose

backbone consists of DNA. Physical entrapment in the dense extracellular network of NETs may certainly be envisioned. Moreover, GO (both small and large sheets) could potentially interact with positively charged histones, a major component of NETs, or with other cationic proteinaceous components of NETs.[40] To confirm the production of NETs, we performed confocal microscopy of neutrophils after incubation with 12.5 μg/mL GO-S or GO-L or 25 nM PMA. We labeled cell samples with anti-NE specific antibodies and counterstained them with DAPI to visualize nuclear chromatin (in cells or extruded as fibers). These studies showed that both small and large GO induced NET production (Figure 2B). To determine whether the effects of small and large GO were quantitatively different, we analyzed the production of NETs by using a well-established assay for the analysis of extracellular NE activity.[39] We observed a pronounced size-dependent effect insofar as large GO was much more effective in triggering NETs than small GO (Figure 2C). PMA (25 nM) was included as a positive control. Thus, it appears that endotoxin-free GO sheets trigger NETs, as demonstrated by several complementary approaches, and that this effect is size dependent, possibly as a result of face-to-membrane interactions that are more characteristic of the larger sheets, whereas the smaller sheets are more readily engulfed.

NETs Are Released in a ROS- and Ca^{2+}-Dependent Manner

Neutrophils are able to "sense" the size of microbes and release NETs selectively in response to large pathogens in a manner dependent on dectin-1, a pattern recognition receptor.[41] We performed experiments with specific inhibitors of dectin-1, but the results did not support a role for dectin-1 in GO-induced NET release (data not shown). Instead, we considered the possibility that GO might trigger the production of NETs through a direct effect on the plasma membrane. First, we asked whether GO-induced NET release requires the production of reactive oxygen species (ROS). Stimulation of neutrophils with PMA led to the original discovery that neutrophils release NETs[14] and to the observation that the production of NETs is linked to a neutrophil cell-death process that is distinct from apoptosis and necrosis and dependent on ROS generation mediated by NADPH oxidase.[42] However, more recent studies have suggested that the requirement for NADPH oxidase activation for NET formation may differ depending on the stimulus.[43,44] Neumann et al.[45] reported that methyl-β-cyclodextrin (MβCD), a cholesterol-depleting agent, triggered the formation of NETs in a manner that was independent of NADPH oxidase (i.e., insensitive to pharmacological inhibition using diphenylene iodonium [DPI]), in contrast to PMA-triggered NETs. The authors also confirmed that treatment of neutrophils with MβCD yielded distinct changes in the lipid composition of the cells, including a significant reduction of cholesterol, whereas other lipids such as sphingomyelin were only slightly affected.[45] To study the signaling pathway underlying the formation of NETs in GO-exposed cells, we pre-incubated cells with DPI (10 μM) and then added small or large GO, PMA (25 nM), or MβCD (10 mM). We determined NET production by using the NE activity assay. As shown in Figure 4A, DPI blocked PMA-induced production of NETs, as expected, and completely blocked the production of NETs in neutrophils exposed to small GO sheets. However, the formation of NETs in MβCD-treated cells and in cells incubated with large GO was not affected by DPI, indicating that NADPH oxidase activation by GO is size dependent. Hence, whereas small GO sheets appeared to trigger NETs via canonical NADPH oxidase activation, large GO sheets induced NET formation independent of NADPH oxidase, suggesting that neutrophils "sense" the difference between small and large GO sheets in a manner analogous to pathogen sensing.

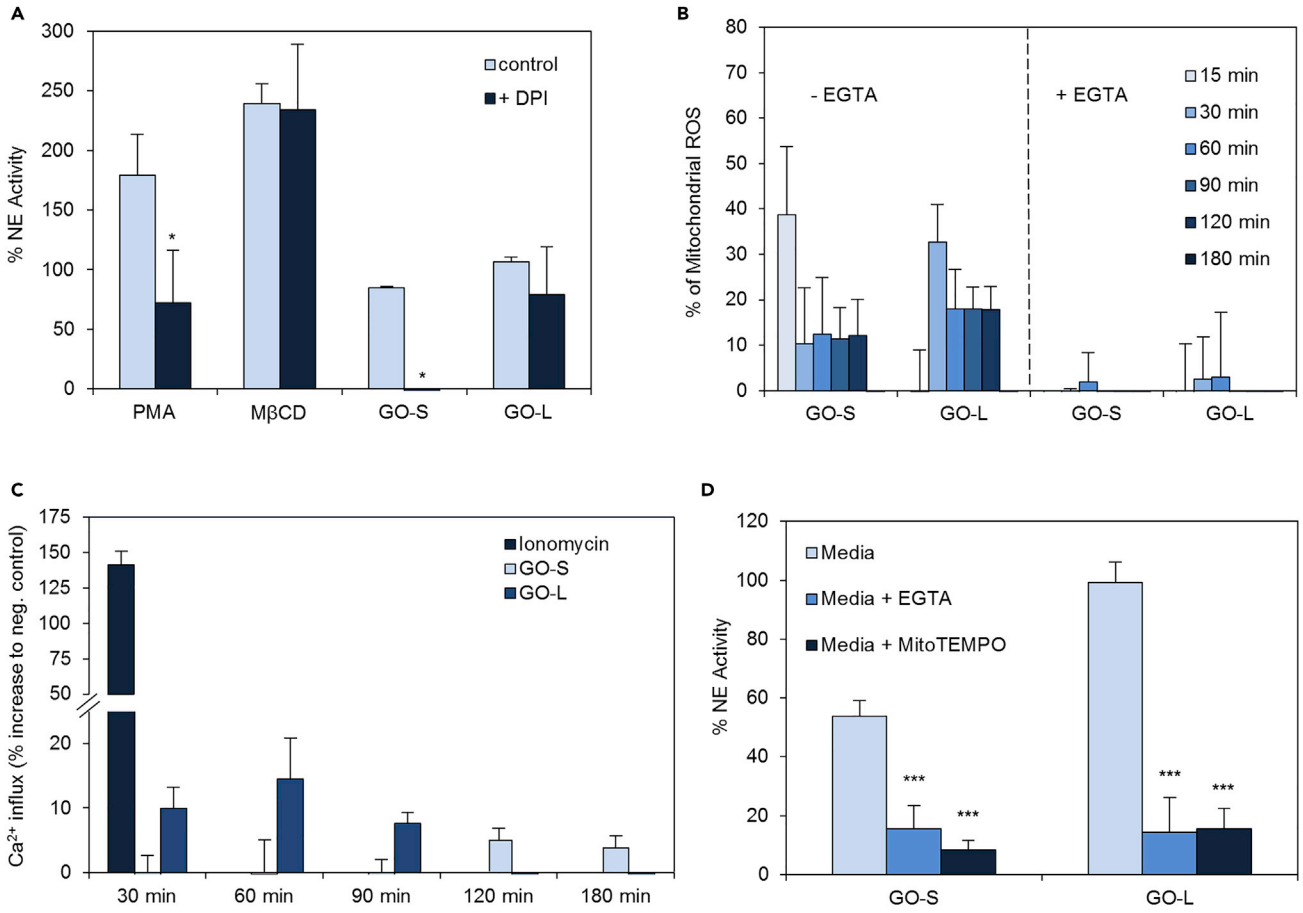

Figure 4. Role of Ca^{2+} and ROS

(A) Cells were pre-incubated or not with DPI (10 μM) and then exposed to PMA (25 nM) or MβCD (10 mM) or GO-L or GO-S (12.5 μg/mL), and NET production was monitored by the NE assay. *$p < 0.05$.

(B) GO-triggered mitochondrial ROS production in neutrophils in the presence or absence of the calcium-chelating agent, EGTA (10 mM). Cells were incubated with GO-S or GO-L (12.5 μg/mL). ROS detection was performed with MitoSOX, a sensor for mitochondrial superoxide.

(C) Cells were incubated with GO-L or GO-S (12.5 μg/mL), and intracellular Ca^{2+} levels were determined with the Fluo-4 Direct Calcium Assay Kit. The Ca^{2+} ionophore, ionomycin (1 μM) was used as positive control.

(D) GO-triggered production of NETs as shown by extracellular NE activity was reduced by EGTA (10 mM) and MitoTEMPO (10 μM), a mitochondria-targeted antioxidant. ***$p < 0.001$.

Cells may also produce ROS in the absence of NADPH oxidase activation, and mitochondrial ROS production was recently shown to play a role in some forms of NETosis.[46] We therefore investigated whether GO elicited mitochondrial ROS production by using MitoSOX, a fluorogenic probe that selectively targets mitochondria and is oxidized by superoxide. These experiments showed that both small and large GO triggered rapid (within 15–30 min) mitochondrial superoxide production (Figure 4B). Calcium overload is known to lead to mitochondrial permeability transition with the production of superoxide, ultimately resulting in the demise of the cell.[47] Furthermore, the calcium ionophore, A23187, triggers NETosis with the production of mitochondrial ROS.[46] We therefore reasoned that mitochondrial ROS production could transpire downstream of calcium influx into the cells. Indeed, as shown in Figure 4C, exposure to GO triggered calcium influx into the cells, with an early response peaking at 60 min for GO-L and a delayed (120 min) and more subdued response to GO-S. Furthermore, calcium chelation using ethylene glycol-bis(β-aminoethyl ether)-*N*,*N*,*N*′,*N*′-tetraacetic acid (EGTA) prevented mitochondrial superoxide

production in neutrophils exposed to GO-S and GO-L (Figure 4D). We also found that pre-incubation of neutrophils with EGTA (10 mM), to prevent calcium signaling, or with the mitochondria-targeted antioxidant, MitoTEMPO (10 μM), resulted in a significant reduction in the production of NETs by GO-S and GO-L (Figure 4D). Together, these results demonstrate that GO-triggered release of NETs in primary human neutrophils is dependent on calcium influx and mitochondrial ROS production. Furthermore, small GO sheets engaged NET formation dependent on NADPH oxidase, whereas micrometer-sized GO appeared to trigger NETs exclusively through a pathway independent of NADPH oxidase; however, both small and large GO triggered neutrophil cell death.

Plasma Membrane Lipid Perturbations Elicited by GO

Lipid rafts are cholesterol- and sphingolipid-rich plasma membrane microdomains with important roles in cell signaling.[48] MβCD efficiently depletes membrane cholesterol and disrupts lipid rafts.[45] In light of the fact that MβCD and GO both triggered NET formation (Figure 4A), we asked whether GO also has an impact on lipid rafts in neutrophils. First, we confirmed that MβCD caused a disruption of lipid rafts in neutrophils by staining with Alexa-Fluor-594-conjugated cholera toxin B subunit (CTXB), a commonly used lipid raft marker that binds glycosphingolipids.[49] As shown in Figure S4A, MβCD induced a loss of lipid raft integrity, as expected. Moreover, using filipin III, a probe for sterol location in biological membranes,[50] we noted a concomitant reduction in cholesterol content in neutrophil membranes upon treatment with MβCD (Figures S4B and S4C). Next, we incubated neutrophils with small or large GO (12.5 μg/mL) and then performed confocal imaging of Alexa-Fluor-594-conjugated CTXB. We found that GO-L caused a disruption of lipid raft domains, as demonstrated by a loss of CTXB staining (Figure S5). We also observed a reduction in filipin III staining in cells exposed to GO-L (Figure S4C), but not in response to PMA (data not shown). On the basis of these results, we hypothesized that GO might deplete or otherwise alter plasma membrane lipids in a manner similar or analogous to that of MβCD and thereby trigger the formation of NETs. To characterize lipid changes caused by exposure to large GO, we performed ToF-SIMS imaging mass spectrometry. ToF-SIMS is a highly sensitive surface analytical method suitable for probing lipid membrane changes on the very surface of the cell, as well as in the depth of the lipid membrane of a cell.[51] High-mass-resolution ToF-SIMS spectra comparing control and GO-exposed neutrophils revealed a multitude of lipid changes primarily in negative ion polarity (Figure 5A), the main effect being a general decrease in cholesterol and highly elevated levels of oxidized cholesterol species such as 7-ketocholesterol ($C_{27}H_{43}O_2$, $[M - H]^-$), hydroxycholestanedione ($C_{27}H_{44}O_3$, $[M - H]^-$) and alliosterol ($C_{27}H_{46}O_4$, $[M - H]^-$) (full spectra in Figure S6). High lateral resolution imaging showed that these areas of abundant oxidized cholesterol could be imaged at approximately 500 nm spatial resolution in the GO-exposed neutrophils but not in control neutrophils (Figures 5B–5K). The membrane structure appeared to be strongly affected by GO, as demonstrated by membrane protrusions in the ion images from PO_3^- at m/z = 79 and $[C_4H_6PO_6]^-$ at m/z = 181. We also used ToF-SIMS to examine neutrophils exposed to MβCD and PMA. MβCD could clearly be seen to extract cholesterol from the plasma membrane, given that the cholesterol signal at $C_{27}H_{45}O$ was reduced by more than half in comparison with control neutrophils (Figure S7A). MβCD also appeared to cause a general disturbance of the neutrophil plasma membrane. PMA induced oxidation of cholesterol but to a higher degree than GO (Figure S7B), whereas the overall membrane structure remained unaffected. High-mass-resolution ToF-SIMS spectra of control neutrophils and neutrophils exposed to GO (12.5 μg/mL), MβCD (10 mM), and PMA (25 nM) are shown in Figure 6. GO caused a marked depletion of the cholesterol signal at $[C_{27}H_{45}O]$.

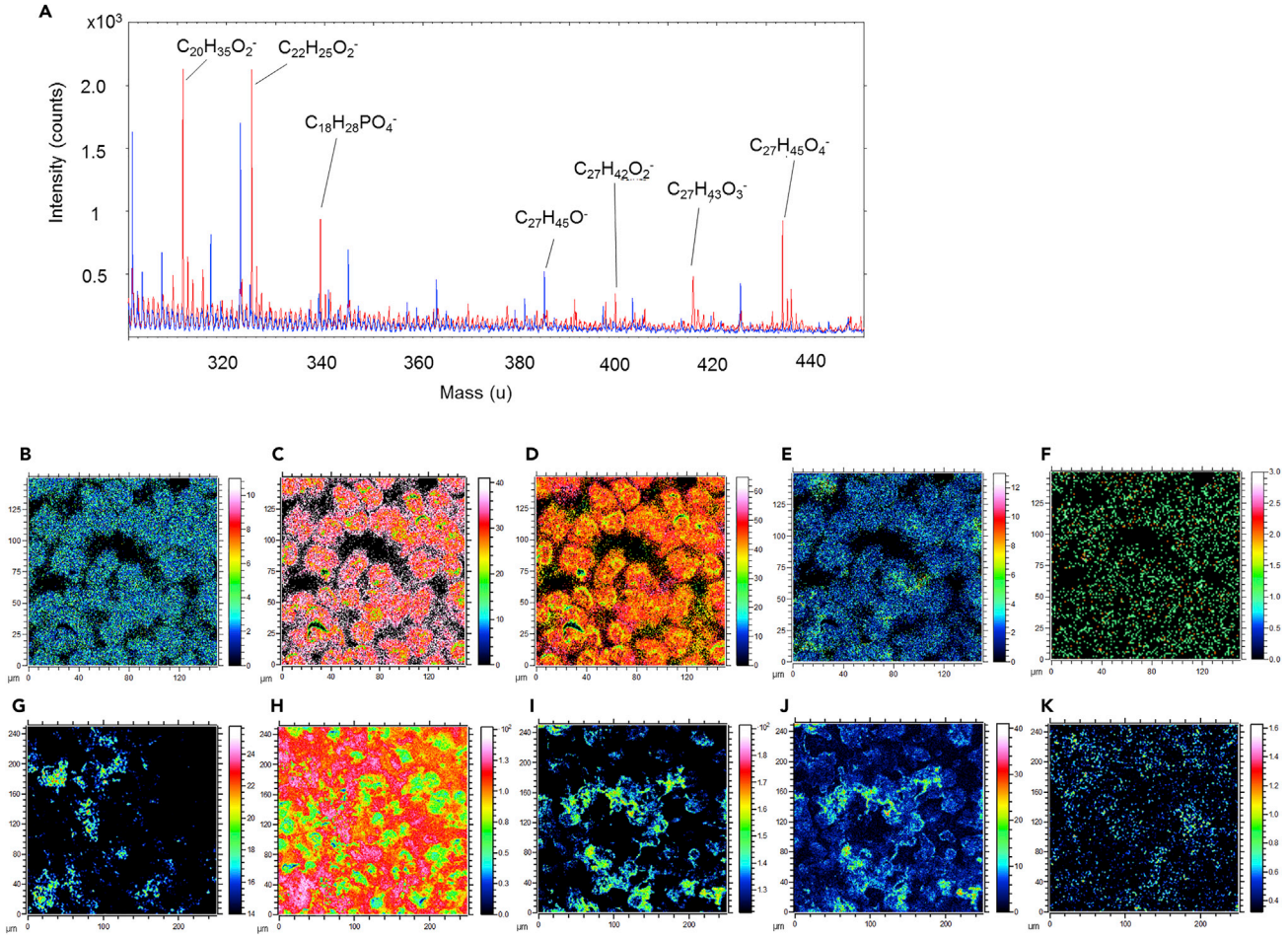

Figure 5. ToF-SIMS Analysis of GO-Exposed Cells

(A) High-mass-resolution ToF-SIMS spectra comparing control (blue) and GO-exposed (red) neutrophils in negative-ion mode. Major differences could be seen in the mass range of 300–450 *m/z*, where oxidized cholesterol species such as 7-ketocholesterol [$C_{27}H_{43}O_2$], hydroxycholestanedione [$C_{27}H_{44}O_3$], and alliosterol [$C_{27}H_{46}O_4$] were elevated in GO-exposed cells. See also Figure S6 for full spectra for control and treated cells.

(B–K) High-spatial-resolution ToF-SIMS images showing control neutrophils (B–F) and GO-exposed neutrophils (G–K) in negative-ion mode. Neutrophils were exposed to GO-L (12.5 μg/mL) for 1 hr. The panels show (B) carbon [C] at *m/z* = 12; (C) CN^- (proteins) at *m/z* = 26; (D) PO_3^- at *m/z* = 79; (E) [$C_4H_6PO_6$] at *m/z* = 181; (F) sum of oxidized cholesterol species [$C_{27}H_{43}O_2$], [$C_{27}H_{44}O_3$], and [$C_{27}H_{46}O_4$] at *m/z* = 399, 415, and 433, respectively; (G) GO as indicated by [$C_3/C_4/C_5/C_6$]; (H) CN^- (proteins) at *m/z* = 26; (I) PO_3 at *m/z* = 79; (J) [$C_4H_6PO_6$] at *m/z* = 181; and (K) sum of oxidized cholesterol species [$C_{27}H_{43}O_2$], [$C_{27}H_{44}O_3$], and [$C_{27}H_{46}O_4$] at *m/z* = 399, 415, and 433, respectively. Field of view: 150 × 150 μm at a pixel resolution of 580 nm. Refer to Figure S7 for MβCD- and PMA-treated neutrophil samples.

This was also the case for MβCD-exposed neutrophils where the cholesterol signal at [$C_{27}H_{45}O$] was depleted. The latter finding was expected because MβCD caused a depletion of cholesterol (Figure S4). PMA treatment, on the other hand, did not affect the cholesterol signal but elicited a higher expression of several other lipid species such as the c16:0 and c18:0 fatty acids $[C_{16}H_{31}O_2]^-$ and $[C_{18}H_{35}O_2]^-$ (Figure 6).

Using ToF-SIMS 3D imaging, we could examine the distribution and lipid changes in the depth of the lipid membrane (Figure 7). The z-corrected 3D ToF-SIMS showed the distribution of GO, CN^-, PO_3^-, and $C_4H_6PO_6$, clearly indicating the structure of the neutrophils (Figures 7A–7D). ToF-SIMS depth profile intensity data from GO-exposed neutrophils in negative-ion mode showed that the oxidation of cholesterol takes place at the very outer layers of the membrane associated with

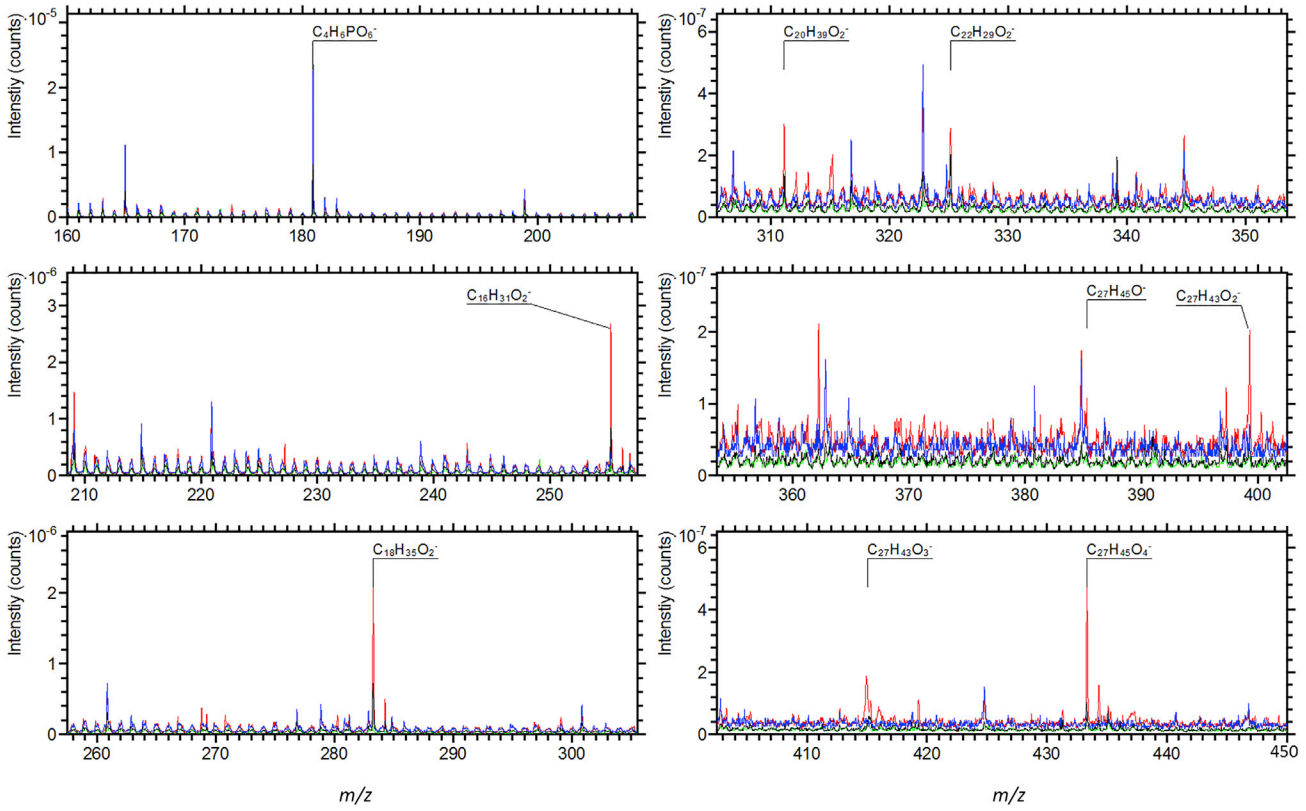

Figure 6. ToF-SIMS Analysis of GO-Exposed Cells

High-mass-resolution ToF-SIMS spectra comparing control neutrophils (blue), GO-exposed neutrophils (black), MβCD-exposed neutrophils (green), and PMA-exposed neutrophils (red) in negative-ion mode. The ion dose for each experiment ranged between 6.3×10^{11} and 9.9×10^{11} ions/cm^2. Region of interest spectra from the cells were selected from fields of view ranging from 150 × 150 μm to 250 × 250 μm for the removal of any influence from the substrate. The spectra were normalized to the total ion dose for each experiment. Control cells showed the highest abundance of $[C_4H_6PO_6]^-$, a signal that can be attributed to the phosphatidylcholine and phosphatidylserine components of the cell membranes. For the GO-exposed neutrophils (black), a depletion of the cholesterol signal at $[C_{27}H_{45}O]$ could be clearly distinguished, whereas MβCD (green) caused an almost complete depletion of the cholesterol signal. PMA treatment (red) did not affect the cholesterol signal but elicited a higher expression of several other lipid species such as the fatty acids $[C_{16}H_{31}O_2]^-$ and $[C_{18}H_{35}O_2]^-$.

phospholipids, as well as deeper in the neutrophil associated with CN^- (Figure 7E). This result was confirmed by a 3D reconstruction of the depth profile data (Figure 7F) where the GO and oxidized cholesterols $[C_{27}H_{43}O_2]^-$, $[C_{27}H_{44}O_3]^-$, and $[C_{27}H_{46}O_4]^-$ are found (Figures 7H and 7I) and can be seen to be associated with the membrane-related ion species $[C_4H_6PO_6]$ (Figure 7G). These results show that the oxidation caused by GO mainly takes place at the outer cell membrane, as well as in other cholesterol-containing lipid membranes in the cell.

Antioxidant Prevents Cholesterol Oxidation and NET Formation

Recent studies have demonstrated that the presence of carbon radicals plays a critical role for the antibacterial effects of GO with induction of lipid oxidation.[52] We asked whether the effects of GO on plasma membrane lipids (especially cholesterol) could be explained by material-induced rather than cell-induced chemical changes. To this end, we performed electron paramagnetic resonance (EPR) measurements followed by assessment of pro-oxidative capacity by using the DCF assay, which measures the conversion of 2′,7′dichlorodihydrofluorescein (H_2DCF) to a fluorescent 2′,7′-dichlorofluorescein (DCF) derivative.[52] We found that both the large and small GO sheets have a single resonance peak where g = 2.004 and 2.005,

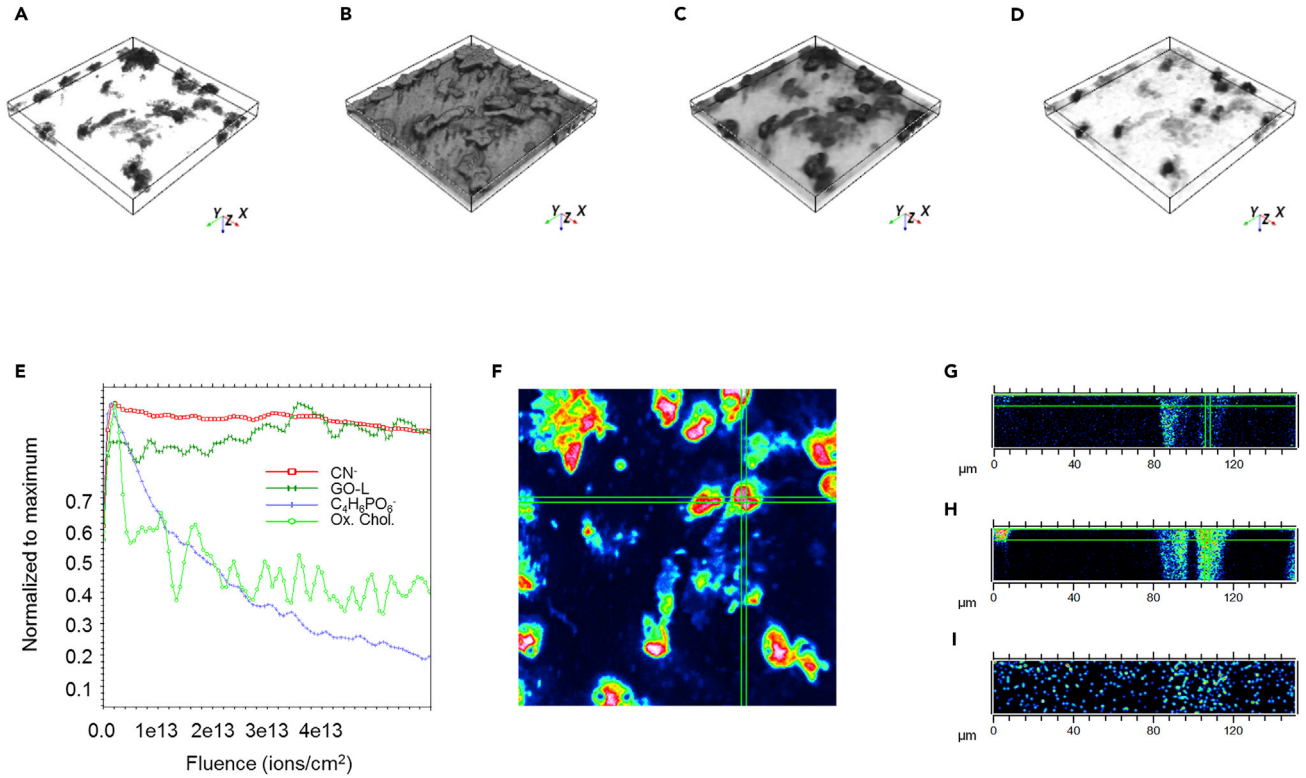

Figure 7. ToF-SIMS 3D Imaging of GO-Exposed Neutrophils

(A–D) Z-corrected 3D ToF-SIMS images based on depth profiling data show the 3D distribution of (A) GO with C_4^- as marker, (B) CN^- at m/z = 26, (C) PO_3^- at m/z = 79, and (D) $[C_4H_6PO_6]$ at m/z = 181.

(E) ToF-SIMS depth profile intensity data from GO-exposed neutrophils (12.5 μg/mL for 1 hr) in negative-ion mode. The red line indicates CN^- at m/z = 26, the dark green line indicates GO, and the blue line denotes $[C_4H_6PO_6]$ at m/z = 181; oxidized cholesterols $[C_{27}H_{43}O_2]$, $[C_{27}H_{44}O_3]$, and $[C_{27}H_{46}O_4]$ at m/z = 399, 415, and 433, respectively, are identified by the light-green line. C_{60}^{+++} ions were used for sputtering a crater of 400 × 400 μm and analyzing an area of 151 × 151 μm with Bi_3^+ ions. We then took a region of interest of the cells to create the depth profile to avoid contribution from the cell substrate. The total dose density of the experiment was 1.13 × 10^{15} ions/cm^2; 4 × 10^{13} ions/cm^2 is shown here with 60 layers out of a total of 1,627, representing the outermost membrane signals.

(F–I) 3D reconstruction of the depth profile data. In (F) is the slice used for reconstructing images in (G)–(I) with four x and y slices, ten z scans, and 35 scans of the depth profiling data per step. $[C_4H_6PO_6]$ at m/z = 181 (G), GO (H), and the average filtered sum of oxidized cholesterols $[C_{27}H_{43}O_2]$, $[C_{27}H_{44}O_3]$, and $[C_{27}H_{46}O_4]$ at m/z = 399, 415, and 433, respectively, (I) show the distribution of GO associated with the oxidized cholesterol species.

respectively, which confirmed the existence of π-conjugated single carbon radicals on the GO surface (Figure 8A), in line with previous publications.[52,53] Furthermore, both GO samples were found to cause oxidation of H_2DCF within 10 min of incubation, although GO-L was a more efficient oxidizing agent than GO-S at lower concentrations (12.5 and 25 μg/mL) (Figure 8B). Next, we asked whether GO-S or GO-L could directly oxidize cholesterol in an acellular setting. Cholesterol (100 mg/mL in ethanol) was drop casted onto glass slides and incubated with GO (12.5 and 50 μg/mL), and samples were then analyzed by ToF-SIMS. We analyzed cholesterol $[C_{27}H_{45}O]^-$ and oxidized cholesterol species, such as 7-ketocholesterol $[C_{27}H_{43}O_2]^-$, hydroxycholestanedione $[C_{27}H_{44}O_3]^-$, and alliosterol $[C_{27}H_{46}O_4]^-$, but could not find any evidence of cholesterol oxidation by GO (Figures 8C and 8D). This result suggested to us that the cholesterol oxidation that was seen in the plasma membrane of neutrophils exposed to GO was likely a multi-step reaction requiring both material-induced and cellular processes. To further probe the mechanism of cholesterol oxidation and its importance for the generation of NETs, we performed experiments in which neutrophils were pre-incubated with

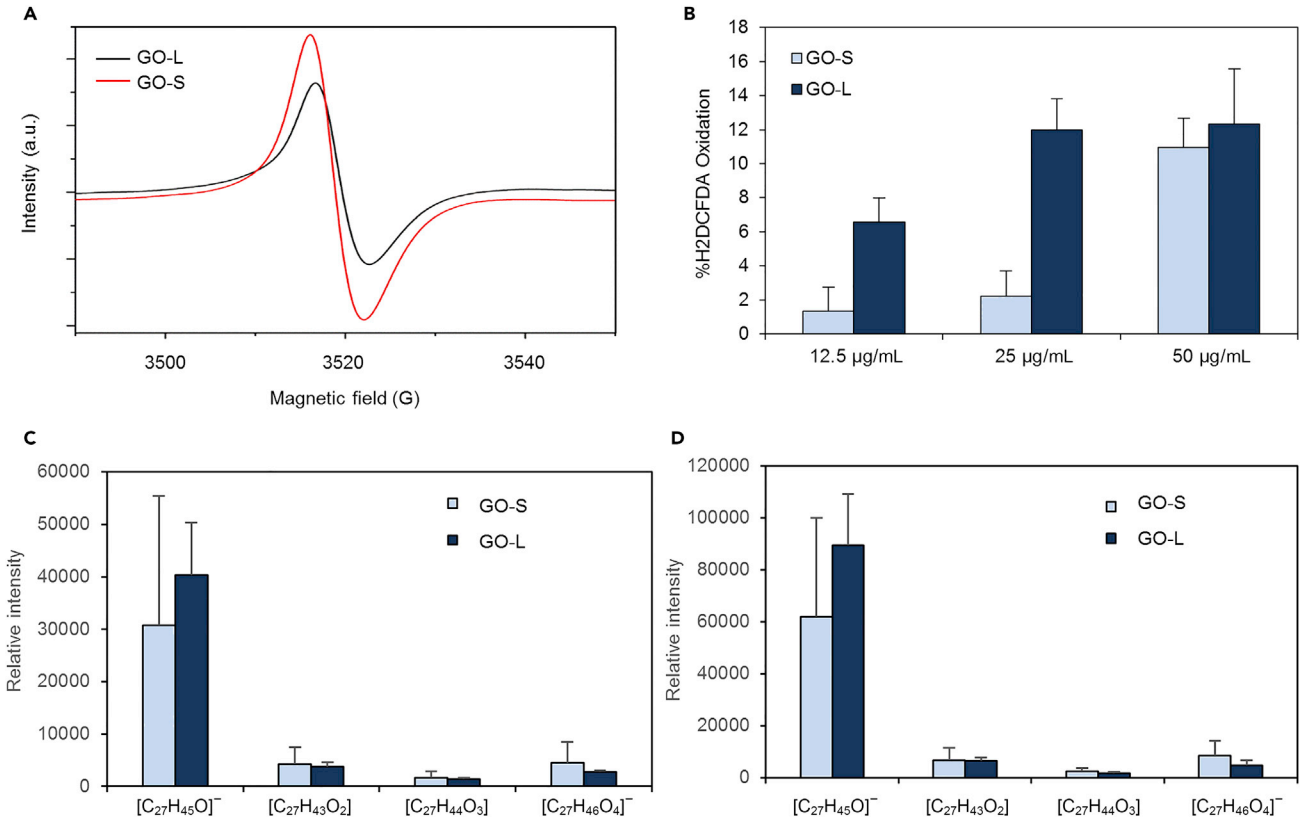

Figure 8. Carbon Radicals and Acellular Oxidation

(A) EPR signature of GO-S (red) and GO-L (black) shows a single peak, confirming the presence of carbon radicals. Measurements were taken with 1.5 mg of dry GO sheets of GO-S and GO-L.

(B) DCF assay showing direct oxidation of H_2DCF (10 μM) by increasing concentrations of GO-S and GO-L at 10 min of co-incubation. Data are expressed as the percent increase over control H_2DCF.

(C and D) ToF-SIMS analysis of potential cholesterol oxidation by GO (acellular conditions). Cholesterol $[C_{27}H_{45}O]^-$ and oxidized cholesterol species such as 7-ketocholesterol $[C_{27}H_{43}O_2]^-$, hydroxycholestanedione $[C_{27}H_{44}O_3]^-$, and alliosterol $[C_{27}H_{46}O_4]^-$ are shown. Relative intensity data from high-mass-resolution ToF-SIMS spectra compare samples exposed for 3 hr to GO-S (light blue) or GO-L (dark blue) at (C) 12.5 μg/mL and (D) 50 μg/mL. See also Figure S8 for a schematic summary.

Trolox (6-hydroxy-2,5,7,8-tetramethylchroman-2-carboxylic acid), a vitamin E analog that acts as a potent antioxidant.[54] We hypothesized that if cholesterol oxidation is required for the formation of NETs, then Trolox would prevent NET formation by virtue of its protective effect against lipid oxidation. After pre-incubation with Trolox (500 μM), we incubated the cells with GO and analyzed them by using the NE assay for quantification of NETs and by confocal microscopy and ToF-SIMS to determine the impact on lipid raft integrity and cholesterol oxidation, respectively. We found that Trolox significantly reduced the generation of NETs (Figure 9A) and that Trolox also appeared to protect against lipid raft disruption induced by exposure to GO (Figure S5). Furthermore, Trolox was shown to reduce cholesterol oxidation in the plasma membrane of neutrophils exposed to GO (Figures 9B–9E). It has been noted that varying the molecular environment of model membranes may affect the ToF-SIMS analysis of phospholipids in such membranes.[55] However, as antioxidant treatment decreased the amount of oxidized cholesterol that could be detected by ToF-SIMS, the changes in lipid oxidation that we recorded in neutrophil membranes do not appear to be a matrix effect, but instead an effect caused by GO.

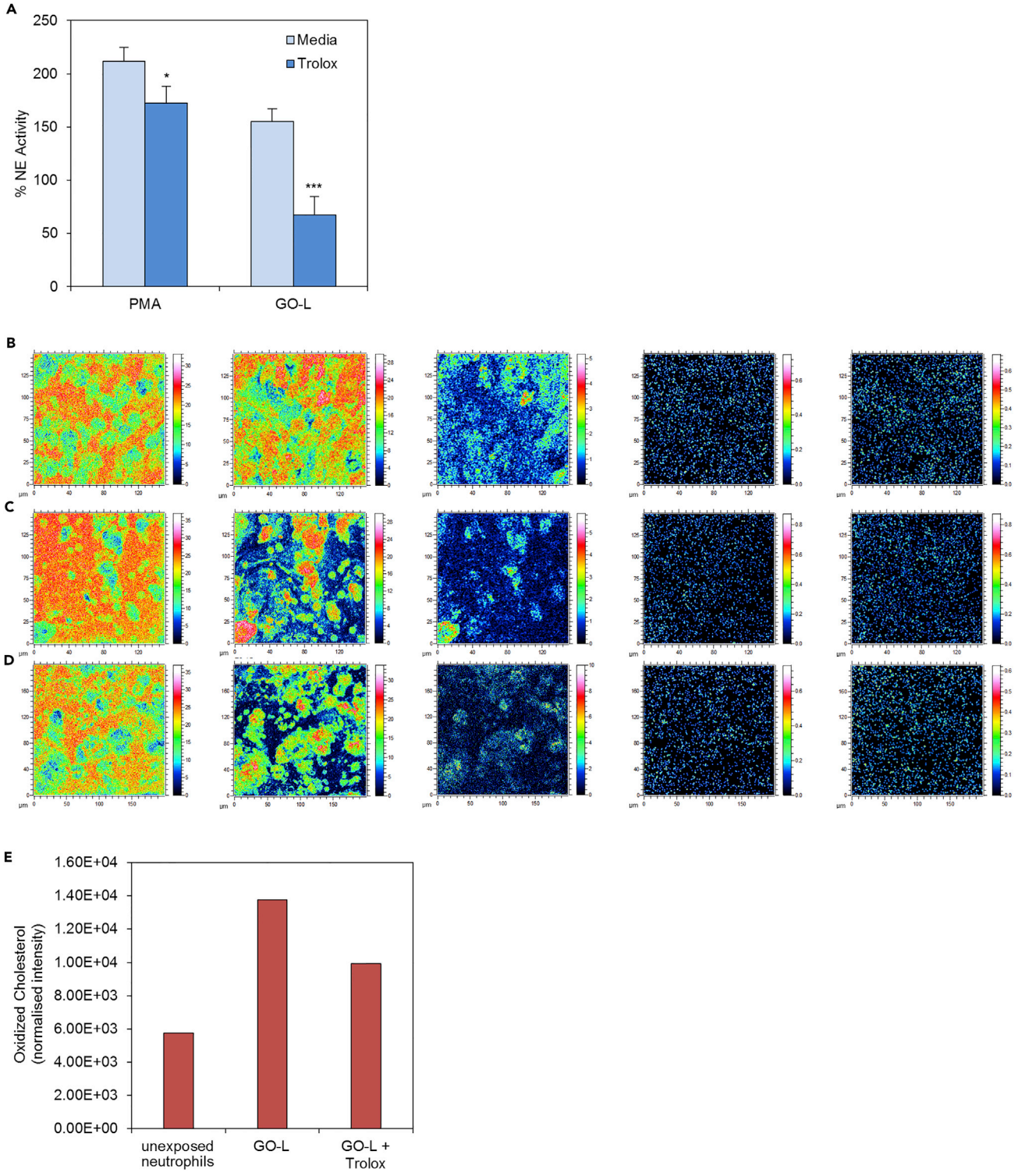

Figure 9. Trolox Reduces Cholesterol Oxidation

(A) Production of NETs as determined by extracellular NE activity in neutrophils exposed to PMA (25 nM) or GO-L (12.5 μg/mL) for 2 hr with or without pre-incubation for 30 min with the antioxidant Trolox (500 μM). Data are shown as the percent increase over the control sample. *$p < 0.05$; ***$p < 0.001$. (B–D) High-spatial-resolution ToF-SIMS images showing control neutrophils (B), GO-L-exposed neutrophils (C), and Trolox-treated, GO-L-exposed neutrophils (D) in negative-ion mode. The images show (from left to right) CN^- at $m/z = 26$, PO_3^- at $m/z = 79$, $[C_4H_6PO_6]^-$ at $m/z = 181$, cholesterol

Figure 9. *Continued*

$[C_{27}H_{45}O]^-$ at m/z = 385 (average filtered), and oxidized cholesterol $[C_{27}H_{43}O_2]^-$ at m/z = 399 (average filtered). Field of view: 150 × 150 μm at a pixel resolution of 585 nm for all images.

(E) Sum of oxidized cholesterol species 7-ketocholesterol $[C_{27}H_{43}O_2]^-$, hydroxycholestanedione $[C_{27}H_{44}O_3]^-$, and alliosterol $[C_{27}H_{46}O_4]^-$ are shown by semi-quantitative measurements of high-mass-resolution ToF-SIMS spectra comparing cellular samples. Spectra were normalized to the total ion dose and m/z = 184 (membrane lipid) to account for the number of cells analyzed in each experiment. Values are shown as normalized intensity.

Previous studies have suggested that the presence of 7-ketocholesterol reduces the level of organization in model phospholipid membranes compared with cholesterol.[56] Thus, it is conceivable that cholesterol oxidation could lead to the disruption of lipid raft domains. Interestingly, statins—cholesterol-lowering drugs that inhibit 3-hydroxy 3-methylglutaryl coenzyme A (HMG-CoA) reductase, the rate-limiting enzyme in cholesterol biosynthesis—were also shown to boost the production of NETs by human and murine neutrophils.[57] Hence, lipid raft disruption by MβCD-induced depletion of cholesterol from the cell membrane or through inhibition of cholesterol synthesis or cholesterol oxidation, as shown in the present study, appears to be linked to the production of NETs. Together, our results support a model in which GO, as a result of the presence of carbon radicals, initiates a reaction in the plasma membrane and leads to cholesterol oxidation and a disruption of lipid rafts, which in turn acts as a trigger for the generation of NETs. Trolox, in turn, prevents cholesterol oxidation by scavenging the carbon radicals on GO and/or cellular radicals, thereby preventing NETs.

Conclusions

ToF-SIMS has previously been used for studying lipid changes in cells and tissues and is gaining in use because the technique is able to detect a wide range of molecular species with high chemical specificity without the need for labels or probes.[58,59] For instance, ToF-SIMS has been used for studying alterations of lipids in the plasma membrane of macrophage-like THP.1 cells exposed to silver nanoparticles[60] and detecting polymeric nanoparticles in bone-marrow-derived stromal cells,[61] and it can be used for both 2D and 3D imaging of lipid membrane changes in cells.[62,63] The present study applied ToF-SIMS to elucidate the effects of a graphene-based material on cells. Our data thus show that ToF-SIMS can be used for directly demonstrating lipid alterations in the plasma membrane of GO-exposed neutrophils. Previous studies have suggested, on the basis of computer simulations, that graphene can "wreak havoc" on cell membranes[64] and have predicted that phospholipid extraction from membranes may occur.[27,65] Furthermore, recent work using supported lipid membranes has pointed to a role of the lateral dimensions of GO for lipid membrane interactions.[66] However, direct experimental evidence of lipid extraction and/or lipid oxidation in membranes of bacterial or mammalian cells has been lacking. By using confocal microscopy and SEM, we were able to show that GO, specifically large GO sheets, disrupted lipid raft domains in neutrophils and triggered NETs. Furthermore, by using ToF-SIMS, we observed a lowering of cholesterol and a marked elevation of oxidized cholesterol species in neutrophil membranes upon exposure to large GO sheets. Cholesterol oxidation can occur through non-enzymatic reactions initiated by free radical species and by non-radical ROS such as singlet oxygen, HOCl, and ozone.[67] 7-Ketocholesterol, which we identified in GO-exposed cell membranes, is thought to be produced mainly via non-enzymatic pathways.[68] We propose that GO, because of the presence of carbon radicals, may initiate a reaction leading to cholesterol oxidation (Figure S8). Mitochondrial ROS could contribute to this reaction; in addition, MPO-generated oxidants could perhaps play a role for cholesterol oxidation in neutrophils. However, given that the release of NETs is thought to require NADPH oxidase and/or mitochondrial ROS production[46] as well as MPO,[69] it is difficult to dissect their role(s)

in cholesterol oxidation without impeding NET production. Notably, the pathway of NET formation in neutrophils exposed to large GO sheets is similar to the recently described pathway of Ca^{2+}-induced NETosis[46] mediated by mitochondrial ROS and independent of NADPH oxidase, although the initial trigger is different, whereas the induction of NETs by small GO sheets, albeit less pronounced, appears more similar to the classical PMA-induced NETosis[70] dependent on NADPH oxidase.

The present study revealed a pronounced size-dependent effect insofar as large GO was more effective in triggering NETs than small GO. Besides the influence of lateral dimensions, other parameters could also modulate biological effects of GO such as the oxidation level.[13] Indeed, by varying this parameter, studies have shown that it is possible to alter the biocompatibility of GO after subcutaneous and peritoneal implantation, which is of broad relevance for medical devices.[71] Furthermore, the presence of graphite impurities, not metallic impurities, within CNTs has recently been shown to be responsible for the apparent electrocatalytic properties of these materials, leading to oxidation of various biomolecules.[72] Future studies could aim to explore the effects of varying the degree of oxidation of GO on NET formation *in vitro* or *in vivo*.

In conclusion, the present studies have revealed that endotoxin-free GO triggers size-dependent responses in primary human neutrophils, and our work has identified key elements of the signaling pathway upstream of NET release in GO-exposed cells. These results support the emerging view that the toxicity of GO could be related to its effects on the plasma membrane[25,29,73] and provide direct experimental evidence of lipid perturbations in cells exposed to GO. This does not exclude a role for phagocytosis-associated cellular effects,[74] but the data suggest that large, micrometer-sized GO sheets, in particular, may act directly on the cell membrane. Notably, the adjuvant, alum, was previously shown to trigger responses in DCs by altering membrane lipid structures, demonstrating that not all immune signaling is receptor mediated and implying that the plasma membrane may behave as a sensor for solid structures.[75] In a subsequent report, it was suggested that uric acid crystals also engaged DC membranes and caused redistribution of cholesterol leading to intracellular signaling.[76] The present study has provided evidence that detrimental effects of GO on the plasma membrane of neutrophils lead to NET formation. Importantly, although several studies exist on interactions of GO with macrophages or macrophage-like cell lines,[77,78] there is a lack of information on the impact of graphene-based materials on neutrophils. Unscheduled release of NETs is linked to a plethora of noninfectious conditions, including thrombosis, atherosclerosis, systemic and organ-specific autoimmune diseases, cancer, and acute trauma.[16] On the other hand, the current study has also demonstrated that these effects are reduced by Trolox, a vitamin E analog, suggesting strategies by which to mitigate the adverse effects of GO on neutrophils.

EXPERIMENTAL PROCEDURES

GO Synthesis and Characterization

GO sheets were synthesized according to the modified Hummers' method as previously described.[32] The synthesis was performed under endotoxin-free conditions with a laminar flow hood, water for injection, gloves, non-pyrogenic plastic containers, and depyrogenated glassware.[34] In brief, 0.8 g of graphite flakes (Graflake 9580) obtained from Nacional Grafite (Brazil) were mixed with 0.4 g of sodium nitrate

in a round-bottom flask, and then 18.4 mL of sulfuric acid 99.999% was added slowly to the mixture. After obtaining a homogenized mixture, 2.4 g of potassium permanganate was slowly added, and the mixture was maintained for 30 min; 37 mL of water for injection was added drop-wise because of the violent exothermic reaction, and the temperature was continuously monitored and kept at 98°C for 30 min. The mixture was further diluted with 112 mL of water for injection, and 30% hydrogen peroxide was added for the reduction of the residual potassium permanganate, manganese dioxide, and manganese heptoxide to soluble manganese sulfate salts. The resulting mixture was purified by several centrifugation steps at 9,000 rpm for 20 min until a viscous orange/brown layer of pure GO started appearing on top of the oxidation by-products at pH 6. This GO gel-like layer was extracted carefully with warm water, resulting in large GO (GO-L). Final concentrations ranging between 1 and 2 mg/mL were obtained with a yield of approx. 10%. GO-L was freeze dried, reconstituted in water for injection, sonicated in a bath sonicator (VWR, 80 W) for 5 min, and centrifuged at 13,000 rpm for 5 min at room temperature to prepare small GO (GO-S). The GO samples have been shown to remain stable for more than 1 year.[79] In the present study, all GO samples were used within 1 year of their production. The samples were stored in darkness until experimental use because GO can undergo photo-reduction in sunlight.[80]

Structural properties, i.e., lateral dimension and thickness of the GO samples were studied by optical microscopy, TEM, and AFM. Optical properties such as absorbance and fluorescence were studied by UV-visible (UV-vis) spectroscopy and fluorescence spectroscopy, respectively. Surface properties were studied by Raman spectroscopy and ζ potential measurements. To elucidate the functionalization degree of the GO sheets, we performed TGA. We used XPS to quantify the chemical composition of the GO, the C:O ratio, and the contribution of individual functional groups such as carboxylic acids, carbonyls, and epoxides.

TEM

TEM was performed with a Tecnai 12 BioTwin (Philips/FEI) 100 kV electron microscope. One drop of sample was placed on a formvar-carbon-coated copper grid. Filter paper was used to remove the excess material.

AFM

Lateral dimension and thickness distributions of GO were studied with a multimode AFM in the tapping mode with a J-type scanner, Nanoscope V controller, operating with NanoScope Analysis software (version 1.40) (Veeco, Cambridge, UK) and an OTESPA silicon probe (Bruker, Coventry, UK). Images were taken in air, by depositing 20 μL of 100 μg/mL GO on a freshly cleaved mica surface (Agar Scientific, Essex, UK) coated with poly-L-lysine 0.01% (Sigma-Aldrich, UK) and allowed to adsorb for 5 min. Excess unbound material was removed by washing with Milli-Q water and then allowed to dry in air; this step was repeated once.

Optical Microscopy

Bright-field microscopy using a Zeiss PrimoVert microscope was used for assessing the lateral dimension distribution of GO-L and to verify the size reduction of GO-S.

UV-Vis Spectroscopy

UV-vis absorbance spectra were collected for GO samples (small and large) from 7.5 to 200 μg/mL with a Varian Cary winUV 50 Bio spectrophotometer. Dual-beam mode and baseline correction were used throughout the measurements to scan the peak wavelength and maximum absorbance between 200 and 800 nm.

Fluorescence Spectroscopy

Fluorescence emission spectra were collected for GO samples (small and large) from 75 to 200 μg/mL with an LS-50B PerkinElmer spectrofluorometer at an excitation wavelength of 525 nm and both excitation and emission slits set at 20.

Raman Spectroscopy

Raman spectra were recorded for GO-L and GO-S (20 μL of 100 μg/mL) on glass slides after complete evaporation of water. Measurements were carried out with a Thermo Scientific DXR micro-Raman spectrometer. Spectra were collected with a 50× objective at 633 nm laser excitation and a 25 s exposure time.

Zeta Potential Measurements

Electrophoretic mobility (μ) was measured by Malvern Zetasizer Nano ZS (UK) after dilution of samples with water in disposable Zetasizer cuvettes (Malvern Instruments). Default instrument settings and automatic analysis were used for all measurements, where the μ was converted automatically by the equipment software to ζ potential values, because it is directly related to ζ potential by Henry's equation. All values are triplicate measurements; the values are mean ± SD.

TGA

The weight loss of the GO samples was performed by TGA with a Pyris 6 analyzer (PerkinElmer); 1–2 mg of GO weighed into a ceramic crucible was analyzed from 25°C to 995°C at 10°C/min with a nitrogen flow of 20 mL/min.

XPS

The composition of GO surfaces was studied by XPS at the NEXUS facility (the UK's National EPSRC XPS Users' Service, hosted by nanoLAB in Newcastle-upon-Tyne). XPS was recorded with a Thermo Theta Probe XPS spectrometer with a monochromatic Al K-α source of 1,486.68 eV. The survey XPS spectra were acquired with pass energy (PE) of 200 eV, 1 eV step size, 50 ms dwell time, and averaged over 5 scans. The etching was 90 s. The high-resolution C1s XPS spectra were acquired with PE of 40 eV, 0.1 eV step size, 100 ms dwell time, and averaged over 20 scans. Spectra from insulating samples have been charge corrected by shifting all peaks to the adventitious carbon C1s spectral component binding energy set to 284.6 eV. CasaXPS software was used to process the spectra acquired at NEXUS. For the deconvolution of the different components, the CasaXPS software was used, and the different regions have been assigned according to Nist XPs and lasurface databases: π-π*, 290.9–289.7; O–C=O, 288.8–288.0 eV; C=O, 287.6–286.6 eV; C–O–C, 286.7–286.3 eV; C–OH, 285.9–285.3 eV; C–C and C=C: 284.6 eV.

Characterization of GO Dispersed in Cell Culture Medium

GO samples were incubated (100 μg/mL) for 24 hr at room temperature in RPMI-1640 culture medium (Sigma, UK) supplemented with 2 mM L-glutamine, 100 U/mL penicillin, and 100 mg/mL streptomycin. These suspensions underwent two centrifugation cycles of 30 min at 13,000 rpm and 20°C. After each centrifugation step, the supernatants were discarded, and the GO pellets were gently re-suspended in Milli-Q water. The final reconstituted suspension was subjected to zeta potential measurements by DLS and AFM as described above.

EPR

EPR measurements were obtained with an EMX XBand Bruker spectrometer. The field was calibrated with a standard sample with a known *g* factor (2,2-diphenyl-1-picrylhydrazyl). After lyophilization of the large and small GO samples, approximately 1.5 mg of the

dry GO sheets was placed in an EPR tube. EPR measurements were performed at room temperature with a frequency of 9.867821 and 9.866372 GHz for GO-L and GO-S, respectively, a center field at 3,520 G, and attenuator at 30 dB.

H_2DCF/DCF Acellular Oxidation Assay

GO-S and GO-L were incubated at the indicated concentrations with 25 μM H_2DCF in dH_2O for 10 min (up to 3 hr) at 37°C. DCF fluorescence was measured at an excitation and emission of 485 and 535 nm, respectively (bandwidth Ex and Em ± 20 and 25 nm, respectively), with an Infinite F200 Tecan plate reader (Männendorf, Switzerland). The results are expressed as a percent increase in comparison with the unexposed negative control. GO-S or GO-L alone at the respective concentrations were measured in parallel to quantify the auto-fluorescence at the excitation and emission wavelengths, and the auto-fluorescence of GO was deducted from the samples where GO was incubated with H_2DCF. The results are expressed as an average of eight replicates.

Endotoxin Assessment

GO samples were assessed for endotoxin content with the TNF-α expression test (TET), which enables unequivocal detection of endotoxin with a sensitivity comparable to that of the conventional LAL assay but without any interference with the assay.[34] In brief, PBMCs were isolated from buffy coats obtained from healthy human blood donors (Karolinska University Hospital, Stockholm, Sweden) by density gradient centrifugation.[81] Then, PBMCs were positively selected for CD14 expression with CD14 MicroBeads (Miltenyi Biotech, Bergisch Gladbach, Germany). For obtaining human monocyte-derived macrophages (HMDMs), $CD14^+$ monocytes were cultured in RPMI-1640 cell medium supplemented with 2 mM L-glutamine, 100 IU/mL penicillin, 100 μg/mL streptomycin, and 10% heat-inactivated fetal bovine serum (FBS), supplemented with 50 ng/mL recombinant macrophage colony-stimulating factor for 3 days in 96-well plates. HMDMs were exposed to GO (50 μg/mL) or to bacterial LPS (Sigma-Aldrich) in the presence or absence of the specific LPS inhibitor, polymyxin B (10 μM) (Sigma-Aldrich), and TNF-α secretion was measured at 24 hr of exposure with a Human TNF-α ELISA Kit purchased from Abcam (Sweden).

Neutrophil Isolation and Culture

Neutrophils were isolated from buffy coat of healthy human blood donors (Karolinska University Hospital, Stockholm, Sweden) as previously described.[36] In brief, neutrophils were separated by density gradient centrifugation with Lymphoprep (Axis Shield, Oslo, Norway) and then subjected to gradient sedimentation in a 5% dextran solution and hypotonic lysis of residual erythrocytes. Isolated neutrophils were maintained in phenol red-free RPMI-1640 culture medium (Sigma) supplemented with 2 mM L-glutamine, 100 U/mL penicillin, and 100 μg/mL streptomycin without serum (FBS) in 5% CO_2 at 37°C.

The identity of the blood donors was unknown to the scientists performing the experiments and the Ethical Committee for Human Studies in Stockholm has determined, in the context of a previous study, that no specific approval is required for such studies as the data cannot be traced back to individual donors (protocol 2006/3:8).

Cytotoxicity Assessment

Freshly isolated primary human neutrophils were seeded in 96-well plates in phenol red-free RPMI-1640 cell medium at a density of 1×10^6 cells/mL and exposed to

PMA (Sigma-Aldrich) or small or large GO at the indicated concentrations, or were maintained in cell medium alone (negative control) at 37°C, in a humidified 5% CO_2 incubator. Then, cells were lysed, and total cellular ATP content was quantified with a luminescence-based Cell Viability Kit SL (BioThema, Sweden), according to the manufacturer's protocol. Luminescence was detected with an Infinite F200 Tecan plate reader (Männendorf, Switzerland).

TEM

For ultrastructural studies, freshly isolated neutrophils were exposed to 12.5 μg/mL of GO-L or GO-S, or left unstimulated for 2 hr at 37°C. The samples were then fixed with 2.5% glutaraldehyde in 0.1 M phosphate buffer, rinsed in phosphate buffer (PB), and centrifuged. The pellets were then post fixed in 2% osmium tetroxide in 0.1 M PB (pH 7.4) at 4°C for 2 hr, dehydrated in ethanol followed by acetone, and embedded in LX-112 (Ladd, Burlington, VT). Ultrathin sections (~60–80 nm) were cut by a Leica ultracut UCT and contrasted with uranyl acetate followed by lead citrate and examined with in Tecnai 12 Spirit Bio TWIN electron microscope (Fei, Eindhoven, the Netherlands) at 100 kV. Digital images were captured with a Veleta camera (Olympus Soft Imaging Solutions GmbH, Münster, Germany).

NET Formation

SEM

SEM to visualize NETs was performed as described previously.[40] In brief, freshly isolated neutrophils were seeded at a density of 1 × 10^6 cells/ml on poly-L-lysine-coated coverslips. After incubation with 25 nM PMA or 12.5 μg/mL of small and large GO for 3 hr at 37°C, samples were fixed with 2.5% glutaraldehyde in 0.1 M PB. Samples were then rinsed briefly in dH_2O and placed in 70% ethanol for 10 min followed by 95% ethanol for 10 min, absolute ethanol for 15 min, and finally in acetone. Samples were dried with a critical point dryer (Balzer, CPD 010, Lichtenstein) and CO_2. After drying, mounting on an aluminum stub, and coating with carbon (Bal-Tec MED 010, Lichtenstein), SEM was carried out. Samples were analyzed with an Ultra 55 field emission microscope (Zeiss, Oberkochen, Germany) at 3 kV.

NE Activity

NE activity in the cell culture supernatants was analyzed as described before.[40] Freshly isolated neutrophils were seeded at a density of 1 × 10^6 cells/mL in phenol red-free RPMI-1640 medium in 96-well plates, 200 μL/well, and incubated with 25 nM PMA, 6.25 μg/mL or 12.5 μg/mL of GO-S and GO-L, 10 mM MβCD (Sigma), or left unstimulated for 3 hr at 37°C. In some experiments, before the exposure to GO, neutrophils were pre-incubated for 30 min with 10 μM DPI or 500 μM Trolox, a water-soluble analog of vitamin E, both from Sigma. After exposure, the cell medium was collected through repetitive pipetting and centrifuged at 1,600 rpm for 6 min. Then, 150 μL of supernatant was retrieved and used for assessing NE activity. In brief, 50 μL of sample was incubated with 0.3 U/μL of DNaseI (QIAGEN) for 15 min at room temperature, then 50 μL of assay buffer (Tris 0.1 M, NaCl 0.5 M [pH 8]) containing *N*-(methoxysuccinyl)-Ala-Ala-Pro-Val-4-nitroanilide (Sigma) at a final concentration of 200 μM was added. After incubation for 3 hr at room temperature, absorbance at 405 nm was measured with an Infinite F200 Tecan plate reader (Männendorf, Switzerland). To understand the role of mitochondrial ROS, neutrophils were pre-incubated with MitoTEMPO (10 μM) for 30 min in RPMI-1640 cell culture medium and then exposed to 12.5 μg/mL of GO-S and GO-L for 3 hr at 37°C 5% CO_2. In addition, to assess the role of (extracellular) calcium, neutrophils were exposed to GO as indicated above, in the presence or absence of EGTA (10 mM).

Confocal Microscopy to Visualize NETs

Freshly isolated neutrophils were seeded at a density of 1 × 10^6 cells/mL on poly-L-lysine-coated coverslips in a 24-well plate in the presence or absence of 25 nM PMA or 12.5 μg/mL of GO-S/GO-L and cells were cultured for 3 hr at 37°C. After incubation, fixation in 2% paraformaldehyde solution for 30 min was performed, followed by 30 min blocking with 2% BSA in PBS solution. Staining with primary rabbit antibody against NE (Calbiochem, San Diego, CA) was performed for 1 hr at room temperature at 1:300 in 2% BSA in PBS, followed by staining with secondary fluorescein isothiocyanate (FITC)-labeled anti-rabbit secondary antibody (Sigma) for 45 min at room temperature at 1:500 in 2% BSA in PBS. Slides were then mounted with ProLong Gold Antifade Mountant with DAPI (Thermo Scientific) and visualized with a ZEISS LSM510META confocal microscope (Carl Zeiss, Oberkochen, Germany).

Lipid Raft and Cholesterol Detection

Freshly isolated neutrophils were pre-incubated for 30 min with or without Trolox (500 μM), then seeded at a density of 1 × 10^6 cells/mL in phenol red-free RPMI-1640 medium in a 96-well plate, 200 μL/well, and incubated with 25 nM PMA, 12.5 μg/mL GO-S and GO-L, 10 mM MβCD (Sigma), or left unstimulated for 1 hr at 37°C. After the exposure, the cell medium was removed, and the cells were fixed according to the instructions in the Cholesterol Assay Kit (Abcam) and stained for 1 hr with filipin III dye provided with the kit. After further washing, filipin III fluorescence was measured at an excitation and emission of 360 and 465 nm, respectively (bandwidth Ex and Em ± 35 and 35 nm, respectively), with an Infinite F200 Tecan plate reader (Männendorf, Switzerland). For membrane cholesterol content assessment, freshly isolated neutrophils were pre-incubated for 30 min with or without Trolox (500 μM), followed by 1 hr exposure with GO or MβCD at the indicated concentrations. Cells were then stained with the Cholesterol Assay Kit (Abcam) according to the manufacturers' instruction. This assay makes us of filipin III, the predominant isomer of filipin, which is widely used as a probe for sterol location in biological membranes. For the study of lipid rafts,[82] cells were either pre-incubated for 30 min with or without Trolox (500 μM) and then exposed for 1 hr to GO or MβCD at the indicated concentrations. Cells were then fixed and stained with CTXB (Recombinant)-Alexa Fluor 594 Conjugate (Thermo Fisher Scientific, Sweden) for 45 min at room temperature. Slides were mounted with ProLong Gold Antifade Mountant with DAPI (Thermo Scientific) and visualized with a ZEISS LSM510META confocal microscope (Carl Zeiss, Oberkochen, Germany).

Calcium Measurements

The intracellular calcium (Ca^{2+}) level in neutrophils was measured with a Fluo-4 Direct Calcium Assay Kit (Invitrogen). Freshly isolated neutrophils were incubated at 37°C in a water bath for 45 min in the pre-warmed (37°C) Fluo-4 Direct calcium buffer containing 5 mM probenecid and Fluo-4 Direct calcium reagent supplied with the Fluo-4 Direct Calcium Assay Kit (Thermo Fisher Scientific, Sweden) and RPMI-1640 cell culture medium in 1:1 ratio according to the manufacturers' instructions. After incubation, this solution was removed by centrifugation at 1,000 rpm, and the cells were washed and re-suspended in cell culture medium. Cells were then exposed to 12.5 μg/mL GO-S and GO-L for the indicated time points in clear-bottom black 96-well plates at a density of 1 × 10^6 cells/mL and 200 μL cell suspension/well at 37°C in a 5% CO_2 incubator. The Ca^{2+} ionophore, ionomycin (1 μM) was used as a positive control. At different exposure time points, the fluorescence intensity of the calcium-sensitive dye was measured at an excitation and emission of 485 and 535 nm, respectively (bandwidth Ex and Em ± 20 and 25 nm,

respectively), with an Infinite F200 Tecan plate reader (Männendorf, Switzerland). The fluorescent intensity measured is directly proportional to the intracellular Ca^{2+} level. The results are expressed as a percent increase in comparison with the unexposed negative control cells.

Mitochondrial ROS Production

Mitochondrial superoxide production was measured by MitoSOX Red reagent (Thermo Fisher Scientific, Sweden), which is a live-cell permeant dye that is rapidly and selectively incorporated in mitochondria. In brief, freshly isolated neutrophils were pre-loaded with 5 μM MitoSOX in PBS for 10 min in a 37°C water bath. Then, the cells were washed to remove the excess unloaded MitoSOX dye and re-suspended in the RPMI-1640 cell culture medium. Cells were then exposed at a density of 10^6 cells/mL and 200 μL cell suspension/well to 12.5 μg/mL of GO-S and GO-L for the indicated time points in the presence or absence of the calcium-chelating agent, EGTA (10 mM) (Sigma). The fluorescence intensity of the MitoSOX Red reagent was measured at an excitation and emission of 540 and 590 nm, respectively (bandwidth Ex and Em ± 24 and 20 nm, respectively), with an Infinite F200 Tecan plate reader (Männendorf). The fluorescent intensity measured is directly proportional to the superoxide produced in the mitochondria of the cells. The results are expressed as a percent increase in comparison with the unexposed negative control cells.

ToF-SIMS

Freshly isolated neutrophils were exposed to 12.5 μg/mL GO-S or GO-L, 25 nM PMA, or 10 mM MβCD indicated and seeded on poly-L-lysine (Sigma)-coated glass slides for 1 hr at 37°C in a 5% CO_2 incubator. After the exposure period, the cells were gently washed with ammonium acetate for 30 s and then air dried for 24 hr in a laminar flow hood as described by Brison et al.[83] For some experiments, cells were pre-incubated with or without Trolox (500 μM) before exposure to GO. The slides were then analyzed by ToF-SIMS for cell membrane lipid compositional changes. ToF-SIMS imaging was performed with a TOF.SIMS V (ION-TOF GmbH, Münster, Germany) equipped with a bismuth liquid metal ion gun.[84] Data were recorded in positive and negative ion modes, and spectra were acquired with Bi^{3+} (25 keV) primary ions. High-mass-resolution images from neutrophils were obtained in high current bunched mode with a pulsed primary ion current of 0.34 pA, and the maximum ion dose density was 1.5×10^{12} ions/cm^2. The burst alignment imaging mode was used for high lateral resolution imaging with approximately 580–970 nm/pixel resolution and a fluence of 3.66×10^{12} ions/cm^2. In total at least three images for each experimental condition were analyzed. The SurfaceLab 6 software (v.6.6, ION-TOF) was used for all spectra and image recording, processing, image analysis, and 3D image analysis.[85] The mass spectra were internally calibrated to signals of $[C]^-$, $[CH]^-$, $[C_2]^-$, $[C_3]^-$ and $[C]^+$, $[CH_2]+$, $[CH_3]^+$, and $[C_5H_{12}N]$ for negative and positive ion mode, respectively. Depth profiling was performed in the non-interlaced mode with C_{60}^{3+} ions at a current of 0.180 nA, sputtering a crater of 400 × 400 μm and analyzing an area of 151 × 151 μm with Bi_3 ions reaching a fluence of 1.14×10^{15} ions/cm^2 and an approximated depth of >800 nm for the full depth profile. In addition, acellular experiments were performed in which cholesterol (100 mg/mL in ethanol) ($C_{27}H_{46}O$; catalog no. C3045, Sigma-Aldrich) was drop casted on glass slides and incubated with GO-S or GO-L at the indicated concentrations for 3 hr. The samples were removed and air dried under sterile conditions in a laminar air flow hood for 18 hr and subjected to analysis of cholesterol oxidation by ToF-SIMS, as described above.

Statistics

Endotoxin testing and cell viability assays were performed with cells isolated from four individual human donors, and each experiment was conducted with three replicate samples. NET formation assays and Ca^{2+} and ROS assays were all performed with cells from three to four individual human donors, and each experiment was conducted with three to six replicates. One-way ANOVA was performed as indicated in the respective figures with post hoc Turkey's multiple-comparison test. *$p < 0.05$; **$p < 0.01$; ***$p < 0.001$.

SUPPLEMENTAL INFORMATION

Supplemental Information includes eight figures and one table and can be found with this article online at https://doi.org/10.1016/j.chempr.2017.12.017.

ACKNOWLEDGMENTS

This work was supported by the European Commission through the GRAPHENE Flagship Project (grant agreement nos. 604391 and 696656 to B.F. and K.K.) and the Swedish Research Council (grant no. 2015-05274 to P.M. and grant no. 2016-02040 to B.F.). We thank A.E. Arranz, A. Fielding, H. Leese, and O.A. Putra for performing EPR measurements and analyzing the data at the National EPR Facility of the University of Manchester.

AUTHOR CONTRIBUTIONS

S.P.M. and B.L. performed *in vitro* experiments; K.H. performed TEM and SEM imaging; N.L. synthesized GO materials; N.L., L.N., and A.F.R. characterized GO materials; P.M. performed ToF-SIMS and analyzed the data; all co-authors contributed to the data analysis and interpretation; B.F. and K.K. supervised the study; B.F. conceived the study and wrote the paper with S.P.M. and B.L.; all co-authors approved the final version.

DECLARATION OF INTERESTS

The authors declare no competing financial interests.

Received: April 24, 2017
Revised: June 6, 2017
Accepted: December 19, 2017
Published: January 25, 2018

REFERENCES AND NOTES

1. Ferrari, A.C., Bonaccorso, F., Fal'ko, V., Novoselov, K.S., Roche, S., Bøggild, P., Borini, S., Koppens, F.H., Palermo, V., Pugno, N., et al. (2015). Science and technology roadmap for graphene, related two-dimensional crystals, and hybrid systems. Nanoscale *7*, 4598–4810.

2. Kostarelos, K., and Novoselov, K.S. (2014). Materials science. Exploring the interface of graphene and biology. Science *344*, 261–263.

3. Joshi, R.K., Alwarappan, S., Yoshimura, M., Sahajwalla, V., and Nishina, Y. (2015). Graphene oxide: the new membrane material. Appl. Mater. Today *1*, 1–12.

4. Bhattacharya, K., Mukherjee, S.P., Gallud, A., Burkert, S.C., Bistarelli, S., Bellucci, S., Bottini, M., Star, A., and Fadeel, B. (2016). Biological interactions of carbon-based nanomaterials: from coronation to degradation. Nanomedicine *12*, 333–351.

5. Park, M.V.D.Z., Bleeker, E.A.J., Brand, W., Cassee, F.R., van Elk, M., Gosens, I., de Jong, W.H., Meesters, J.A.J., Peijnenburg, W.J.G.M., Quik, J.T.K., et al. (2017). Considerations for safe innovation: the case of graphene. ACS Nano *11*, 9574–9593.

6. Shvedova, A.A., Pietroiusti, A., Fadeel, B., and Kagan, V.E. (2012). Mechanisms of carbon nanotube-induced toxicity: focus on oxidative stress. Toxicol. Appl. Pharmacol. *261*, 121–133.

7. Bhattacharya, K., Andón, F.T., El-Sayed, R., and Fadeel, B. (2013). Mechanisms of carbon nanotube-induced toxicity: focus on pulmonary inflammation. Adv. Drug Deliv. Rev. *65*, 2087–2097.

8. Kagan, V.E., Konduru, N.V., Feng, W., Allen, B.L., Conroy, J., Volkov, Y., Vlasova, I.I., Belikova, N.A., Yanamala, N., Kapralov, A., et al. (2010). Carbon nanotubes degraded by neutrophil myeloperoxidase induce less pulmonary inflammation. Nat. Nanotechnol. *5*, 354–359.

9. Shvedova, A.A., Kapralov, A.A., Feng, W.H., Kisin, E.R., Murray, A.R., Mercer, R.R., St Croix, C.M., Lang, M.A., Watkins, S.C., Konduru, N.V., et al. (2012). Impaired clearance and enhanced pulmonary inflammatory/fibrotic response to carbon nanotubes in myeloperoxidase-deficient mice. PLoS One *7*, e30923.

10. Sanchez, V.C., Jachak, A., Hurt, R.H., and Kane, A.B. (2012). Biological interactions of graphene-family nanomaterials: an

interdisciplinary review. Chem. Res. Toxicol. *25*, 15–34.

11. Wang, X., Duch, M.C., Mansukhani, N., Ji, Z., Liao, Y.P., Wang, M., Zhang, H., Sun, B., Chang, C.H., Li, R., et al. (2015). Use of a pro-fibrogenic mechanism-based predictive toxicological approach for tiered testing and decision analysis of carbonaceous nanomaterials. ACS Nano *9*, 3032–3043.

12. Shurin, M.R., Yanamala, N., Kisin, E.R., Tkach, A.V., Shurin, G.V., Murray, A.R., Leonard, H.D., Reynolds, J.S., Gutkin, D.W., Star, A., et al. (2014). Graphene oxide attenuates Th2-type immune responses, but augments airway remodeling and hyperresponsiveness in a murine model of asthma. ACS Nano *8*, 5585–5599.

13. Wick, P., Louw-Gaume, A.E., Kucki, M., Krug, H.F., Kostarelos, K., Fadeel, B., Dawson, K.A., Salvati, A., Vázquez, E., Ballerini, L., et al. (2014). Classification framework for graphene-based materials. Angew. Chem. Int. Ed. *53*, 7714–7718.

14. Brinkmann, V., Reichard, U., Goosmann, C., Fauler, B., Uhlemann, Y., Weiss, D.S., Weinrauch, Y., and Zychlinsky, A. (2004). Neutrophil extracellular traps kill bacteria. Science *303*, 1532–1535.

15. Yipp, B.G., Petri, B., Salina, D., Jenne, C.N., Scott, B.N., Zbytnuik, L.D., Pittman, K., Asaduzzaman, M., Wu, K., Meijndert, H.C., et al. (2012). Infection-induced NETosis is a dynamic process involving neutrophil multitasking in vivo. Nat. Med. *18*, 1386–1393.

16. Jorch, S.K., and Kubes, P. (2017). An emerging role for neutrophil extracellular traps in noninfectious disease. Nat. Med. *23*, 279–287.

17. Schauer, C., Janko, C., Munoz, L.E., Zhao, Y., Kienhöfer, D., Frey, B., Lell, M., Manger, B., Rech, J., Naschberger, E., et al. (2014). Aggregated neutrophil extracellular traps limit inflammation by degrading cytokines and chemokines. Nat. Med. *20*, 511–517.

18. Muñoz, L.E., Bilyy, R., Biermann, M.H., Kienhöfer, D., Maueröder, C., Hahn, J., Brauner, J.M., Weidner, D., Chen, J., Scharin-Mehlmann, M., et al. (2016). Nanoparticles size-dependently initiate self-limiting NETosis-driven inflammation. Proc. Natl. Acad. Sci. USA *113*, E5856–E5865.

19. Bartneck, M., Keul, H.A., Zwadlo-Klarwasser, G., and Groll, J. (2010). Phagocytosis independent extracellular nanoparticle clearance by human immune cells. Nano Lett. *10*, 59–63.

20. Monopoli, M.P., Åberg, C., Salvati, A., and Dawson, K.A. (2012). Biomolecular coronas provide the biological identity of nanosized materials. Nat. Nanotechnol. *7*, 779–786.

21. Tenzer, S., Docter, D., Kuharev, J., Musyanovych, A., Fetz, V., Hecht, R., Schlenk, F., Fischer, D., Kiouptsi, K., Reinhardt, C., et al. (2013). Rapid formation of plasma protein corona critically affects nanoparticle pathophysiology. Nat. Nanotechnol. *8*, 772–781.

22. Ge, C., Du, J., Zhao, L., Wang, L., Liu, Y., Li, D., Yang, Y., Zhou, R., Zhao, Y., Chai, Z., et al. (2011). Binding of blood proteins to carbon nanotubes reduces cytotoxicity. Proc. Natl. Acad. Sci. USA *108*, 16968–16973.

23. Chong, Y., Ge, C., Yang, Z., Garate, J.A., Gu, Z., Weber, J.K., Liu, J., and Zhou, R. (2015). Reduced cytotoxicity of graphene nanosheets mediated by blood-protein coating. ACS Nano *9*, 5713–5724.

24. Kapralov, A.A., Feng, W.H., Amoscato, A.A., Yanamala, N., Balasubramanian, K., Winnica, D.E., Kisin, E.R., Kotchey, G.P., Gou, P., Sparvero, L.J., et al. (2012). Adsorption of surfactant lipids by single-walled carbon nanotubes in mouse lung upon pharyngeal aspiration. ACS Nano *6*, 4147–4156.

25. Sun, C., Wakefield, D.L., Han, Y., Muller, D.A., Holowka, D.A., Baird, B.A., and Dichtel, W.R. (2016). Graphene oxide nanosheets stimulate ruffling and shedding of mammalian cell plasma membranes. Chem *1*, 273–286.

26. Pumera, M. (2016). Graphene oxide stimulates cells to ruffle and shed plasma membranes. Chem *1*, 189–190.

27. Tu, Y., Lv, M., Xiu, P., Huynh, T., Zhang, M., Castelli, M., Liu, Z., Huang, Q., Fan, C., Fang, H., et al. (2013). Destructive extraction of phospholipids from *Escherichia coli* membranes by graphene nanosheets. Nat. Nanotechnol. *8*, 594–601.

28. Chen, J., Zhou, G., Chen, L., Wang, Y., Wang, X., and Zeng, S. (2016). Interaction of graphene and its oxide with lipid membrane: a molecular dynamics simulation study. J. Phys. Chem. C *120*, 6225–6231.

29. Duan, G., Zhang, Y., Luan, B., Weber, J.K., Zhou, R.W., Yang, Z., Zhao, L., Xu, J., Luo, J., and Zhou, R. (2017). Graphene-induced pore formation on cell membranes. Sci. Rep. *7*, 42767.

30. Frost, R., Jönsson, G.E., Chakarov, D., Svedhem, S., and Kasemo, B. (2012). Graphene oxide and lipid membranes: interactions and nanocomposite structures. Nano Lett. *12*, 3356–3362.

31. Liu, X., and Chen, K.L. (2015). Interactions of graphene oxide with model cell membranes: probing nanoparticle attachment and lipid bilayer disruption. Langmuir *31*, 12076–12086.

32. Ali-Boucetta, H., Bitounis, D., Raveendran-Nair, R., Servant, A., Van den Bossche, J., and Kostarelos, K. (2013). Purified graphene oxide dispersions lack *in vitro* cytotoxicity and *in vivo* pathogenicity. Adv. Healthc. Mater. *2*, 433–441.

33. Vallhov, H., Qin, J., Johansson, S.M., Ahlborg, N., Muhammed, M.A., Scheynius, A., and Gabrielsson, S. (2006). The importance of an endotoxin-free environment during the production of nanoparticles used in medical applications. Nano Lett. *6*, 1682–1686.

34. Mukherjee, S.P., Lozano, N., Kucki, M., Del Rio-Castillo, A.E., Newman, L., Vázquez, E., Kostarelos, K., Wick, P., and Fadeel, B. (2016). Detection of endotoxin contamination of graphene based materials using the TNF-α expression test and guidelines for endotoxin-free graphene oxide production. PLoS One *11*, e0166816.

35. Orecchioni, M., Jasim, D.A., Pescatori, M., Manetti, R., Fozza, C., Sgarrella, F., Bedognetti, D., Bianco, A., Kostarelos, K., and Delogu, L.G. (2016). Molecular and genomic impact of large and small lateral dimension graphene oxide sheets on human immune cells from healthy donors. Adv. Healthc. Mater. *5*, 276–287.

36. Fadeel, B., Åhlin, A., Henter, J.-I., Orrenius, S., and Hampton, M.B. (1998). Involvement of caspases in neutrophil apoptosis: regulation by reactive oxygen species. Blood *92*, 4808–4818.

37. Yue, H., Wei, W., Yue, Z., Wang, B., Luo, N., Gao, Y., Ma, D., Ma, G., and Su, Z. (2012). The role of the lateral dimension of graphene oxide in the regulation of cellular responses. Biomaterials *33*, 4013–4021.

38. Russier, J., Treossi, E., Scarsi, A., Perrozzi, F., Dumortier, H., Ottaviano, L., Meneghetti, M., Palermo, V., and Bianco, A. (2013). Evidencing the mask effect of graphene oxide: a comparative study on primary human and murine phagocytic cells. Nanoscale *5*, 11234–11247.

39. Farrera, C., and Fadeel, B. (2013). Macrophage clearance of neutrophil extracellular traps is a silent process. J. Immunol. *191*, 2647–2656.

40. Farrera, C., Bhattacharya, K., Lazzaretto, B., Andón, F.T., Hultenby, K., Kotchey, G.P., Star, A., and Fadeel, B. (2014). Extracellular entrapment and degradation of single-walled carbon nanotubes. Nanoscale *6*, 6974–6983.

41. Branzk, N., Lubojemska, A., Hardison, S.E., Wang, Q., Gutierrez, M.G., Brown, G.D., and Papayannopoulos, V. (2014). Neutrophils sense microbe size and selectively release neutrophil extracellular traps in response to large pathogens. Nat. Immunol. *15*, 1017–1025.

42. Fuchs, T.A., Abed, U., Goosmann, C., Hurwitz, R., Schulze, I., Wahn, V., Weinrauch, Y., Brinkmann, V., and Zychlinsky, A. (2007). Novel cell death program leads to neutrophil extracellular traps. J. Cell Biol. *176*, 231–241.

43. Parker, H., Dragunow, M., Hampton, M.B., Kettle, A.J., and Winterbourn, C.C. (2012). Requirements for NADPH oxidase and myeloperoxidase in neutrophil extracellular trap formation differ depending on the stimulus. J. Leukoc. Biol. *92*, 841–849.

44. van der Linden, M., Westerlaken, G.H.A., van der Vlist, M., van Montfrans, J., and Meyaard, L. (2017). Differential signalling and kinetics of neutrophil extracellular trap release revealed by quantitative live imaging. Sci. Rep. *7*, 6529.

45. Neumann, A., Brogden, G., Jerjomiceva, N., Brodesser, S., Naim, H.Y., and von Köckritz-Blickwede, M. (2014). Lipid alterations in human blood-derived neutrophils lead to formation of neutrophil extracellular traps. Eur. J. Cell Biol. *93*, 347–354.

46. Douda, D.N., Khan, M.A., Grasemann, H., and Palaniyar, N. (2015). SK3 channel and mitochondrial ROS mediate NADPH oxidase-independent NETosis induced by calcium influx. Proc. Natl. Acad. Sci. USA *112*, 2817–2822.

47. Orrenius, S., Zhivotovsky, B., and Nicotera, P. (2003). Regulation of cell death: the calcium-apoptosis link. Nat. Rev. Mol. Cell Biol. *4*, 552–565.

48. Lingwood, D., and Simons, K. (2010). Lipid rafts as a membrane-organizing principle. Science *327*, 46–50.

49. Janes, P.W., Ley, S.C., and Magee, A.I. (1999). Aggregation of lipid rafts accompanies signaling via the T cell antigen receptor. J. Cell Biol. *147*, 447–461.

50. Mukherjee, S., Zha, X., Tabas, I., and Maxfield, F.R. (1998). Cholesterol distribution in living cells: fluorescence imaging using dehydroergosterol as a fluorescent cholesterol analog. Biophys. J. *75*, 1915–1925.

51. Nygren, H., and Malmberg, P. (2007). High resolution imaging by organic secondary ion mass spectrometry. Trends Biotechnol. *25*, 499–504.

52. Li, R., Mansukhani, N.D., Guiney, L.M., Ji, Z., Zhao, Y., Chang, C.H., French, C.T., Miller, J.F., Hersam, M.C., Nel, A.E., et al. (2016). Identification and optimization of carbon radicals on hydrated graphene oxide for ubiquitous antibacterial coatings. ACS Nano *10*, 10966–10980.

53. Yang, L., Zhang, R., Liu, B., Wang, J., Wang, S., Han, M.Y., and Zhang, Z. (2014). π-conjugated carbon radicals at graphene oxide to initiate ultrastrong chemiluminescence. Angew. Chem. Int. Ed. *53*, 10109–10113.

54. Barclay, L.R., and Vinqvist, M.R. (1994). Membrane peroxidation: inhibiting effects of water-soluble antioxidants on phospholipids of different charge types. Free Radic. Biol. Med. *16*, 779–788.

55. Sostarecz, A.G., Cannon, D.M., McQuaw, C.M., Sun, S., Ewing, A.G., and Winograd, N. (2004). Influence of molecular environment on the analysis of phospholipids by time-of-flight secondary ion mass spectrometry. Langmuir *20*, 4926–4932.

56. Massey, J.B., and Pownall, H.J. (2005). The polar nature of 7-ketocholesterol determines its location within membrane domains and the kinetics of membrane microsolubilization by apolipoprotein A-I. Biochemistry *44*, 10423–10433.

57. Chow, O.A., von Köckritz-Blickwede, M., Bright, A.T., Hensler, M.E., Zinkernagel, A.S., Cogen, A.L., Gallo, R.L., Monestier, M., Wang, Y., Glass, C.K., et al. (2010). Statins enhance formation of phagocyte extracellular traps. Cell Host Microbe *8*, 445–454.

58. Angerer, T.B., Dowlatshahi Pour, M., Malmberg, P., and Fletcher, J.S. (2015). Improved molecular imaging in rodent brain with time-of-flight-secondary ion mass spectrometry using gas cluster ion beams and reactive vapor exposure. Anal. Chem. *87*, 4305–4313.

59. Malmberg, P., Jennische, E., Nilsson, D., and Nygren, H. (2011). High-resolution, imaging TOF-SIMS: novel applications in medical research. Anal. Bioanal. Chem. *399*, 2711–2718.

60. Haase, A., Arlinghaus, H.F., Tentschert, J., Jungnickel, H., Graf, P., Mantion, A., Draude, F., Galla, S., Plendl, J., Goetz, M.E., et al. (2011). Application of laser postionization secondary neutral mass spectrometry/time-of-flight secondary ion mass spectrometry in nanotoxicology: visualization of nanosilver in human macrophages and cellular responses. ACS Nano *5*, 3059–3068.

61. Kokesch-Himmelreich, J., Woltmann, B., Torger, B., Rohnke, M., Arnhold, S., Hempel, U., Müller, M., and Janek, J. (2015). Detection of organic nanoparticles in human bone marrow-derived stromal cells using ToF-SIMS and PCA. Anal. Bioanal. Chem. *407*, 4555–4565.

62. Fletcher, J.S. (2015). Latest applications of 3D ToF-SIMS bio-imaging. Biointerphases *10*, 018902.

63. Robinson, M.A., Graham, D.J., Morrish, F., Hockenbery, D., and Gamble, L.J. (2015). Lipid analysis of eight human breast cancer cell lines with ToF-SIMS. Biointerphases *11*, 02A303.

64. Dallavalle, M., Calvaresi, M., Bottoni, A., Melle-Franco, M., and Zerbetto, F. (2015). Graphene can wreak havoc with cell membranes. ACS Appl. Mater. Interfaces *7*, 4406–4414.

65. Zhang, L., Xu, B., and Wang, X. (2016). Cholesterol extraction from cell membrane by graphene nanosheets: a computational study. J. Phys. Chem. B *120*, 957–964.

66. Frost, R., Svedhem, S., Langhammer, C., and Kasemo, B. (2016). Graphene oxide and lipid membranes: size-dependent interactions. Langmuir *32*, 2708–2717.

67. Iuliano, L. (2011). Pathways of cholesterol oxidation via non-enzymatic mechanisms. Chem. Phys. Lipids *164*, 457–468.

68. Girotti, A.W. (1998). Lipid hydroperoxide generation, turnover, and effector action in biological systems. J. Lipid Res. *39*, 1529–1542.

69. Metzler, K.D., Goosmann, C., Lubojemska, A., Zychlinsky, A., and Papayannopoulos, V. (2014). A myeloperoxidase-containing complex regulates neutrophil elastase release and actin dynamics during NETosis. Cell Rep. *8*, 883–896.

70. Kenny, E.F., Herzig, A., Krüger, R., Muth, A., Mondal, S., Thompson, P.R., Brinkmann, V., Bernuth, H.V., and Zychlinsky, A. (2017). Diverse stimuli engage different neutrophil extracellular trap pathways. Elife *6*, e24437.

71. Sydlik, S.A., Jhunjhunwala, S., Webber, M.J., Anderson, D.G., and Langer, R. (2015). In vivo compatibility of graphene oxide with differing oxidation states. ACS Nano *9*, 3866–3867.

72. Chng, E.L.K., and Pumera, M. (2012). Nanographite impurities in carbon nanotubes: their influence on the oxidation of insulin, nitric oxide, and extracellular thiols. Chem. Eur. J. *18*, 1401–1407.

73. Zhu, J., Xu, M., Gao, M., Zhang, Z., Xu, Y., Xia, T., and Liu, S. (2017). Graphene oxide induced perturbation to plasma membrane and cytoskeletal meshwork sensitize cancer cells to chemotherapeutic agents. ACS Nano *11*, 2637–2651.

74. Cho, Y.C., Pak, P.J., Joo, Y.H., Lee, H.S., and Chung, N. (2016). In vitro and in vivo comparison of the immunotoxicity of single- and multi-layered graphene oxides with or without pluronic F-127. Sci. Rep. *6*, 38884.

75. Flach, T.L., Ng, G., Hari, A., Desrosiers, M.D., Zhang, P., Ward, S.M., Seamone, M.E., Vilaysane, A., Mucsi, A.D., Fong, Y., et al. (2011). Alum interaction with dendritic cell membrane lipids is essential for its adjuvanticity. Nat. Med. *17*, 479–487.

76. Ng, G., Sharma, K., Ward, S.M., Desrosiers, M.D., Stephens, L.A., Schoel, W.M., Li, T., Lowell, C.A., Ling, C.C., Amrein, M.W., et al. (2008). Receptor-independent, direct membrane binding leads to cell-surface lipid sorting and Syk kinase activation in dendritic cells. Immunity *29*, 807–818.

77. Mukherjee, S.P., Bottini, M., and Fadeel, B. (2017). Graphene and the immune system: a romance of many dimensions. Front. Immunol. *8*, 673.

78. Boraschi, D., Italiani, P., Palomba, R., Decuzzi, P., Duschl, A., Fadeel, B., and Moghimi, S.M. (2017). Nanoparticles and innate immunity: new perspectives on host defence. Semin. Immunol. *34*, 33–51.

79. Rauti, R., Lozano, N., León, V., Scaini, D., Musto, M., Rago, I., Ulloa Severino, F.P., Fabbro, A., Casalis, L., Vázquez, E., et al. (2016). Graphene oxide nanosheets reshape synaptic function in cultured brain networks. ACS Nano *10*, 4459–4471.

80. Hou, W.C., Chowdhury, I., Goodwin, D.G., Jr., Henderson, W.M., Fairbrother, D.H., Bouchard, D., and Zepp, R.G. (2015). Photochemical transformation of graphene oxide in sunlight. Environ. Sci. Technol. *49*, 3435–3443.

81. Kagan, V.E., Gleiss, B., Tyurina, Y.Y., Tyurin, V.A., Elenström-Magnusson, C., Liu, S.X., Serinkan, F.B., Arroyo, A., Chandra, J., Orrenius, S., et al. (2002). A role for oxidative stress in apoptosis: oxidation and externalization of phosphatidylserine is required for macrophage clearance of cells undergoing Fas-mediated apoptosis. J. Immunol. *169*, 487–499.

82. Sun, Y., Orrenius, S., Pervaiz, S., and Fadeel, B. (2005). Plasma membrane sequestration of apoptotic protease-activating factor-1 in human B lymphoma cells: a novel mechanism of chemoresistance. Blood *105*, 4070–4077.

83. Brison, J., Benoit, D.S., Muramoto, S., Robinson, M., Stayton, P.S., and Castner, D.G. (2011). ToF-SIMS imaging and depth profiling of HeLa cells treated with bromodeoxyuridine. Surf. Interface Anal. *43*, 354–357.

84. Fletcher, J.S., Lockyer, N.P., Vaidyanathan, S., and Vickerman, J.C. (2007). TOF-SIMS 3D biomolecular imaging of *Xenopus laevis* oocytes using buckminsterfullerene (C60) primary ions. Anal. Chem. *79*, 2199–2206.

85. Robinson, M.A., Graham, D.J., and Castner, D.G. (2012). ToF-SIMS depth profiling of cells: z-correction, 3D imaging, and sputter rate of individual NIH/3T3 fibroblasts. Anal. Chem. *84*, 4880–4885.